

Chapter 2: Fundamental Properties of Pb-Free Solder Alloys

Carol Handwerker, Purdue University, West Lafayette, Indiana, USA

Ursula Kattner, National Institute of Standards and Technology (NIST),
Gaithersburg, Maryland, USA

Kil-Won Moon, National Institute of Standards and Technology (NIST),
Gaithersburg, Maryland, USA

2.1 Search for a Pb-Free Alternative to Sn-Pb Eutectic

The search for a global Pb-free replacement for Sn-Pb eutectic alloy has been an evolving process as the threat of a regional lead ban became a reality in July 2006. Over the twelve years from 1994 through 2006, the manufacturing, performance, and reliability criteria for Pb-free solder joints have become increasingly complex as relationships between the solder alloy, the circuit board materials and construction, and the component designs and materials have been revealed through widespread experimentation by companies, industrial consortia, and university researchers. The focus of this chapter is to examine the primary criteria used to develop the current generation of Pb-free solder alloys, the tradeoffs made between various properties once these primary criteria were satisfied, and the open questions regarding materials and processes that are as yet unanswered.

2.2 Primary Alloy Design Criteria

The primary alloy design criteria have been developed using Sn-Pb eutectic as a baseline. This approach is eminently logical: the new standard Pb-free alloy replaces Sn-Pb eutectic solder in a wide variety of board designs and microelectronics applications. For more than fifty years, printed wiring boards (PWB) and components had been designed around the behavior of Sn-Pb eutectic solder during circuit board assembly and in use for holding components to the PWBs. This behavior for Pb-free solder was quantified

differently by different research groups over time, as more data on Pb-free solders became available. [1-23]

In the National Center for Manufacturing Science (NCMS) Pb-Free Solder Project completed in 1997, the pass-fail criteria for candidate alloys, as seen in Table 2.1, were created to represent practical restrictions on reflow profiles and maximum temperature, requirements in thermomechanical fatigue life and strength, wetting and oxidation of the molten solder alloy. [1-4]

Table 2.1. Pass-Fail Criteria used by the NCMS Pb-Free Solder Project [1-4]

Solder Property	Definition	Acceptable Levels
Liquidus Temperature	Temperature at which solder alloy is completely molten.	$< 225^{\circ}\text{C}$
Pasty Range	Temperature difference between solidus and liquidus temperatures; temperature range where the alloy is part solid and part liquid.	$< 30^{\circ}\text{C}$
Wettability	A wetting balance test assesses the force resulting when a copper wire is immersed in and wetted by a molten solder bath. A large force indicates good wetting, as does a short time to attain a wetting force of zero and a short time to attain a value of two-thirds of the maximum wetting force.	$F_{\max} > 300 \mu\text{N}$ $t_0 < 0.6 \text{ s}$ $t_{2/3} < 1 \text{ s}$
Area of Coverage	Assesses the coverage of the solder on Cu after a typical dip test.	$> 85\%$ coverage
Drossing	Assesses the amount of oxide formed in air on the surface of molten solder after a fixed time at the soldering temperature.	Qualitative scale
Thermo-mechanical Fatigue	Cycles-to-failure for a given percent failed of a test population based on a specific solder-joint and board configuration, compared to eutectic Sn-Pb.	Some percentage, usually $> 50\%$
Coefficient of Thermal Expansion (CTE)	Thermal expansion coefficient of the solder alloy is the fraction change of length per $^{\circ}\text{C}$ temperature change. Value used for comparison was CTE of solder alloy at room temperature.	$< 2.9 \times 10^{-5}/^{\circ}\text{C}$
Creep	Stress required at room temperature to cause failure in 10,000 minutes.	$> 3.4 \text{ MPa}$
Elongation	Total percent elongation of material under uniaxial tension at room temperature.	$>> 10\%$

By 1999, the WEEE and RoHS Directives led NEMI to establish a less quantitative, but no less restrictive, set of criteria. [15-16] The NEMI alloy was designed to:

- Have a melting point as close to Sn-Pb eutectic as possible
- Be eutectic or very close to eutectic
- Contain no more than three elements (ternary composition)
- Avoid using existing patents, if possible (for ease of implementation)
- Have the potential for reliability equal to or better than Sn-Pb eutectic.

All research groups agreed that there were no “drop-in” replacement alloys for Sn-Pb eutectic. Application of these criteria led to the NEMI choice of the Sn-Ag-Cu system, and specifically to Sn-3.9Ag-0.6Cu ($\pm 0.2\%$) in the Sn-Ag-Cu (SAC) family of alloys as the most promising surface mount alloy solution.

Over the last five years, a worldwide consensus has developed that the general-purpose lead-free alloy is from the Sn-Ag-Cu ternary family. The Solderotec research organization specified a range of compositions Sn-(3.4-4.1)Ag-(0.5-0.9)Cu. The EU consortium project on Improved Design Life and Environmentally Aware Manufacturing of Electronics Assemblies by Lead-Free Soldering (IDEALS) in the European Union recommended the near eutectic alloy Sn-3.8Ag-0.7Cu. [11-14] (Note that all compositions are expressed as Sn-vX-yZ, where the “X” and “Z” are alloying elements in Sn, with the composition being “v” mass fraction*100 of element X, “y” mass fraction*100 of element “Z”, and remainder being Sn; the quantity mass fraction*100 is abbreviated as ‘wt.%’.) While numerous other ternary, quaternary and quinary lead-free alloys were investigated by large Japanese OEM’s, the Japanese industry has moved over time toward the JEITA (Japan Electronics and Information Technology Industries Association) recommended alloy of Sn-3.0Ag-0.5Cu alloy, partly due to concerns over patent issues. (19-22)

Widespread cross-licensing of nearly all the tin-silver-copper family of solder alloys worldwide has meant that alloy selection within the SAC system is now driven primarily by overall performance in product applications and cost of Ag as an alloying agent to solder paste and bar. As is discussed below, the differences in terms of manufacturing and reliability among this full range of SAC alloys are generally believed to be small, based on available melting and reliability data. In the next sections we present the fundamental thermodynamic properties that distinguish Sn-Pb eutectic alloys from Pb-free alloys, with an emphasis on SAC alloys, and relate these differences to the microstructures that are produced when these alloys are used for circuit board assembly (Figure 2.1a-b) and to their behavior in manufacturing and in mechanical property and reliability testing.

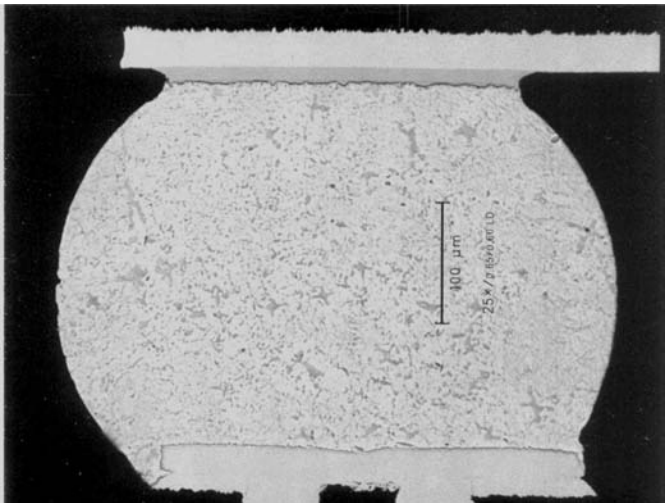


Fig. 2.1a. Characteristic shapes and microstructures of 169 CSP Solder Joints from NEMI Project on Pb-Free Assembly. (a) Sn-Pb alloy cross section

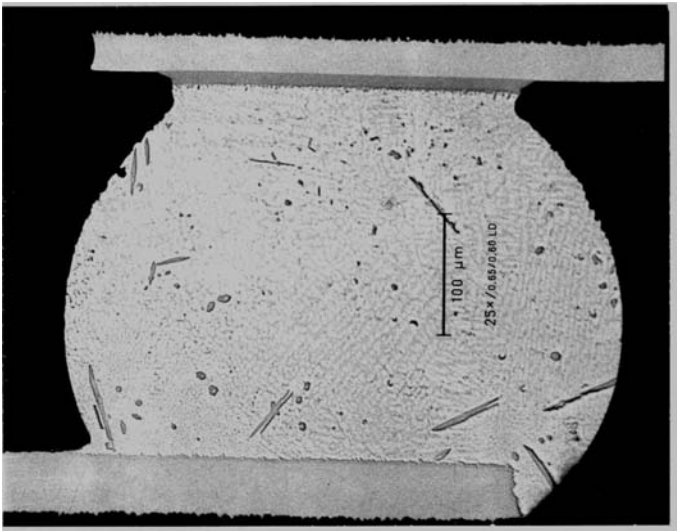


Fig. 2.1b. Characteristic shapes and microstructures of 169 CSP Solder Joints from NEMI Project on Pb-Free Assembly. (b) Sn-3.9Ag-0.6Cu alloy cross section

2.3 Solder Alloy Solidification and Microstructural Development

During their life cycles, from assembly through use in products, solder alloys undergo a wide range of phase transformations that change their compositions, their properties, and the compositions and properties of the materials they contact. Solder alloys melt, then wet and react with the board and component lead materials, sometimes causing significant dissolution of board and component lead materials. As the solder is cooled, the solid phases that form and their morphologies depend on the cooling rate and the relative ease of nucleation of solid phases in the melt and on pre-existing phases.

Solder alloys may exhibit metastable phase formation during solidification as well as microstructural coarsening and reactions with board substrates and component lead materials in the solid state. During product use, the solubilities and the distribution of phases change as a result of thermomechanical fatigue. In terms of the effect of solder alloy composition on the ability to assembly PWBs, some of these phase transformations are clearly identifiable and straightforward to analyze, particularly their melting behavior relative to Sn-Pb eutectic. Others require the full scope of materials science concepts and characterization tools to understand. The phase transformation and interface phenomena involved and typical characterization tools and methods used in solder alloy design are listed in Table 2.2.

2.4 Melting Behavior

2.4.1 Alloy Thermodynamics

The melting behavior of lead-free solder alloys has been, from the beginning, judged against the Sn-Pb system. The Sn-Pb phase diagram (Figure 2.2) is a simple binary eutectic phase diagram characterized by a liquid phase and two solid phases, each with substantial solid solubility. The eutectic composition is Sn-37Pb with a eutectic temperature of 183°C, a reduction of melting temperature (T_l) by almost 50°C from pure Sn at 232°C. The microstructure of Sn-37Pb on solidification is frequently used in metallurgy textbooks as an example of a classic eutectic structure, with its intermixed Sn and Pb solid solution phases.

Without exception, all Pb-free solders considered as candidates to replace Sn-Pb eutectic have been based on Sn modified with additional alloying elements. Using Sn as a base metal, alloying additions have been sought to reduce the liquidus temperature from 232°C while keeping the temperature

Table 2.2. Phase transformation and interface phenomena important for Pb-free solder alloy systems

Phase transformation or interface phenomenon	Property being evaluated	Characterization tool	Measurement signature of phase transformation
Melting, solidification, and phase transformation behavior	Thermodynamic properties of equilibrium phase transformations, including transformation temperatures, compositions	CALPHAD software tools, such as ThermoCalc ¹ , producing calculated phase diagrams	
Melting behavior	Temperatures where various phases begin to melt and where melting is complete	Differential scanning calorimetry (DSC), differential thermal analysis (DTA)	Endothermic peaks associated with melting of each phase
Solidification behavior	Temperatures where various phases begin to form from the melt during cooling	Differential scanning calorimetry (DSC), differential thermal analysis (DTA)	Exothermic peaks associated with phase formation
	Existence of metastable phase formation – stable phases do not nucleate easily	Differential scanning calorimetry (DSC), differential thermal analysis (DTA)	Exothermic peak well below equilibrium solidus temperatures followed by rapid rise in sample temperature up to equilibrium transformation temperature; i.e. recalescence

¹ In this chapter commercial products or trade names are identified for completeness, their use does not imply an endorsement by NIST.

	Existence of metastable phase formation – slow diffusion in solidifying phase leads to composition gradients in solid and non-equilibrium amounts of remaining phases	Differential scanning calorimetry (DSC), differential thermal analysis (DTA)	Exothermic peak well below equilibrium solidus temperatures indicating Scheil effect active during solidification
Microstructures of solid phases – including reaction interfaces between phases	Phases forming during transformations	Optical microscopy, transmission electron microscopy (TEM), scanning electron microscopy (SEM), electron probe microanalysis (EPMA)	Contrast differences in polished cross sections or as-formed structures; in SEM, TEM, and EPMA, composition maps; in TEM, diffraction characteristic of specific phases
		X-ray powder diffraction	Diffraction patterns characteristic of different phases
Wetting and solderability	Conditions for wetting of liquid solder on different substrates	Sessile drop experiments and wetting balance tests	Contact angle and force/time, respectively, as a function of alloy composition, substrate and its condition, flux, and other wetting conditions

difference between solidus and liquidus temperatures as small as possible, even using a eutectic alloy if possible. The thermodynamic characteristics of Sn with other alloying agents can be understood by considering the Sn-Bi, Sn-Ag, Sn-Sb and similar binary phase diagrams. (Binary alloy phase diagrams can also be found in the ASM Binary Alloy Phase Diagram Handbook. [24] Kattner et al. give an extensive discussion of the binary and ternary phase diagrams and sources for solder alloy phase diagrams. [25-26])

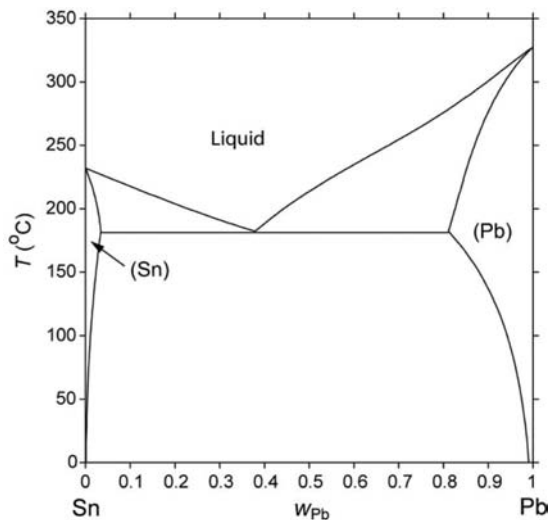


Fig. 2.2. Sn-Pb phase diagram.

In the simple Sn-Bi eutectic phase diagram (Figure 2.3), there is significant solid solubility of Bi in Sn, up to 22 wt% Bi in Sn at the eutectic temperature of 139°C. The liquidus temperature decreases with increasing Bi concentration from 232°C for pure Sn to 139°C at Sn-58Bi. The solidus temperature decreases with increasing Bi concentration from 232°C for pure Sn to 139°C at Sn-22Bi. Alloying elements that display significant solid solubility also exhibit significantly lower liquidus temperatures and eutectic temperatures than those with little solid solubility. Diagrams of this type include Sn-Zn (Figure 2.4) and Sn-Cd. This behavior is in contrast to the Sn-Ag diagram (Figure 2.5). There is negligible solid solubility of Ag in solid Sn. The liquidus temperature decreases from 232°C for pure Sn to 221°C at Sn-3.5Ag. The hypoeutectic solidus line is essentially a vertical line close to pure Sn. This behavior is characteristic of Sn-Cu (Figure 2.6), Sn-Ni (Figure 2.7), and Sn-Au (Figure 2.8).

The third characteristic phase diagram is illustrated by the Sn-Sb system (Figure 2.9). The Sn-Sb system contains a peritectic at the Sn-rich side of the phase diagram, leading to an increase in liquidus temperature with increasing Sb concentration. The phase field for tin, marked “Sn” on the left indicates significant solubility of Sb in Sn at temperatures above approximately 100°C. The Sn-In binary system (Figure 2.10) is slightly more complicated: in addition to the liquid and the two terminal solid solution phases, the Sn-In binary system contains two intermediate phases, both forming through peritectic reactions from the liquid and one of the terminal solution phases. At a temperature of 120°C, a liquid of Sn-51In decomposes by a eutectic reaction into the two intermediate phases.

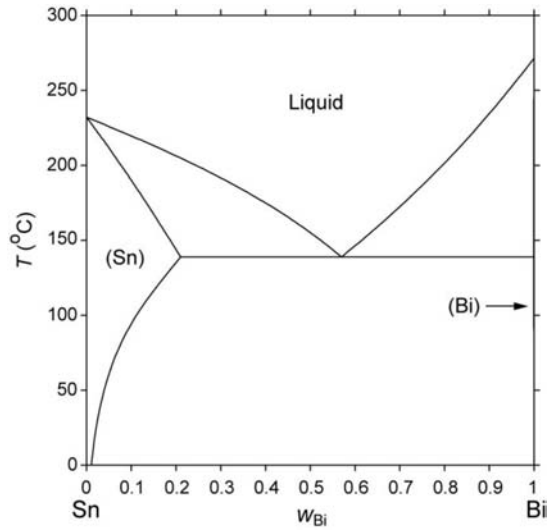


Fig. 2.3. Sn-Bi phase diagram.

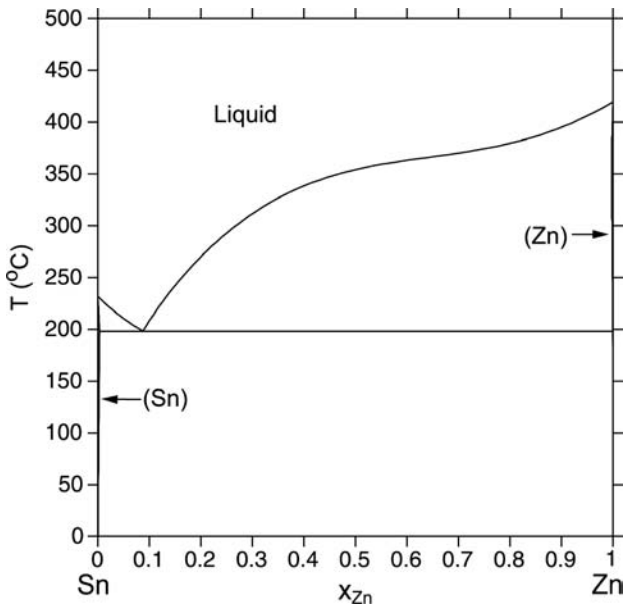


Fig. 2.4. Sn-Zn phase diagram.

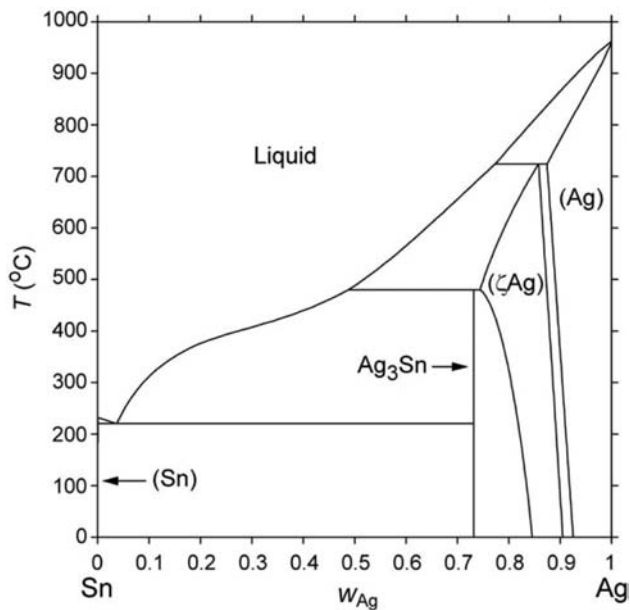


Fig. 2.5. Sn-Ag phase diagram.

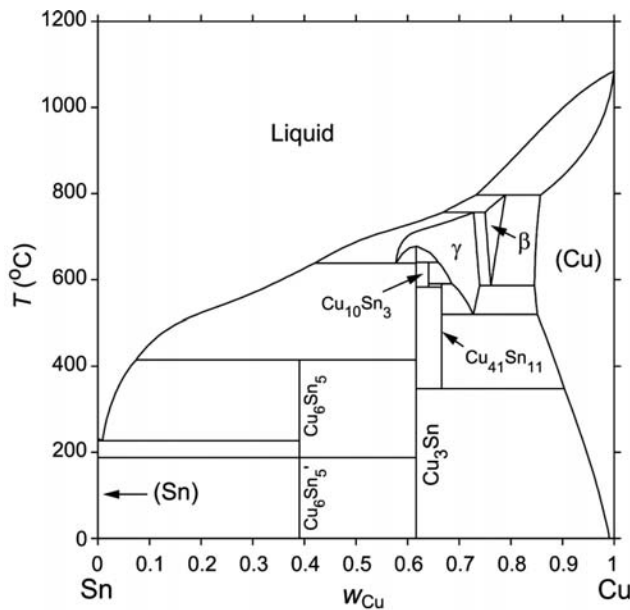


Fig. 2.6. Sn-Cu phase diagram.

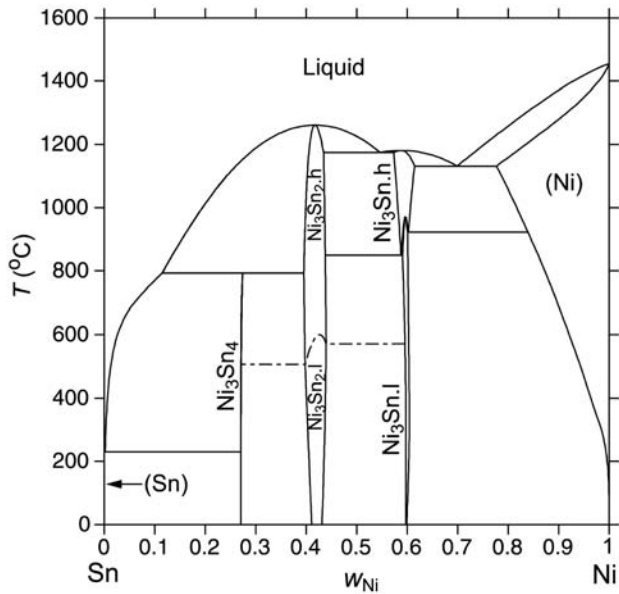


Fig. 2.7. Sn-Ni phase diagram.

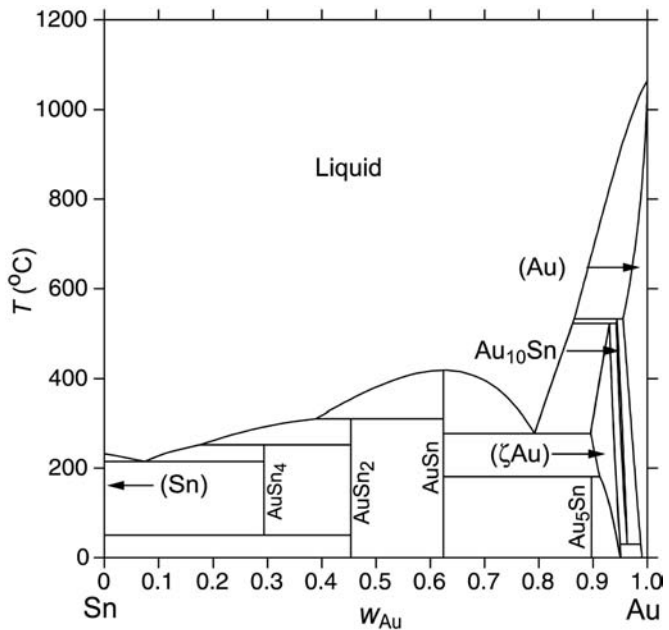


Fig. 2.8. Sn-Au phase diagram.

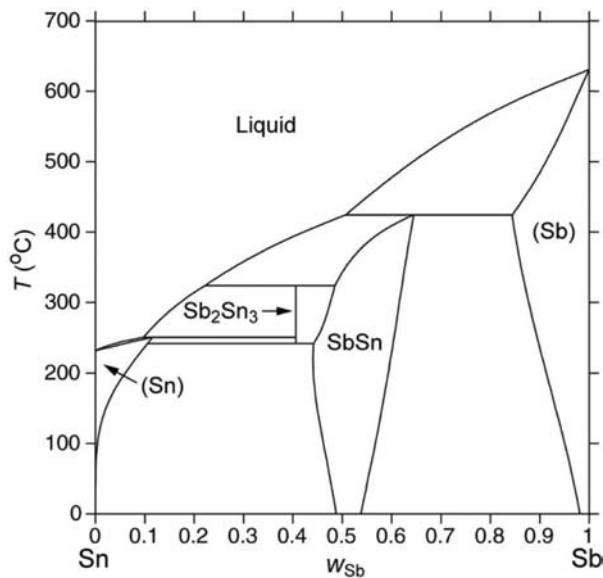


Fig. 2.9. Sn-Sb phase diagram.

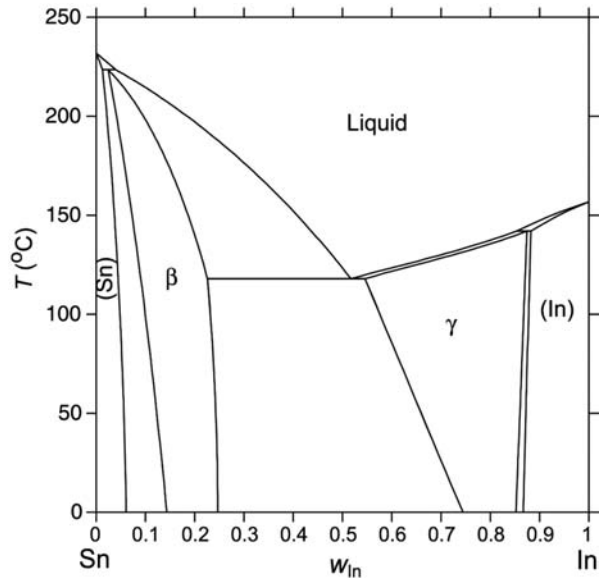


Fig. 2.10. Sn-In phase diagram.

These binary phase diagrams can be used to understand the melting behavior possible with ternary and quaternary Pb-free solder alloys. The primary alloy design criteria described above required (1) the liquidus temperature to be as close as possible to 183°C, in order to avoid changing manufacturing processes, materials, and infrastructure, (2) the solidus temperature to be as close as possible to the liquidus temperature, to avoid tombstoning phenomenon and fillet lifting (which are described further in this chapter), and (3) the solidus temperature significantly higher than the solder joint's maximum operating temperature. Binary and ternary eutectics obviously meet the second criterion; however, eutectic Sn-based alloys tend to fall into two temperature regimes with respect to the other two criteria. The high temperature, Sn-rich eutectics are Sn-0.9Cu (227°C), Sn-3.5Ag (221°C), Sn-0.16Ni (231°C), Sn-10Au (217°C), Sn-9Zn (199°C), and Sn-3.5Ag-0.9Cu (217°C) (Figure 2.11). The low temperature eutectic solders are Sn-58Bi (139°C), Sn-59Bi-1.2Ag (138°C) (Figure 2.12), Sn-59Bi-.04Cu (139°C) (Figure 2.13) and Sn-51In (120°C). (The eutectic in the Sn-Cd binary system of 177°C is close to ideal as a substitute for Sn-Pb from the point of view of melting point. However, Cd is highly toxic.)

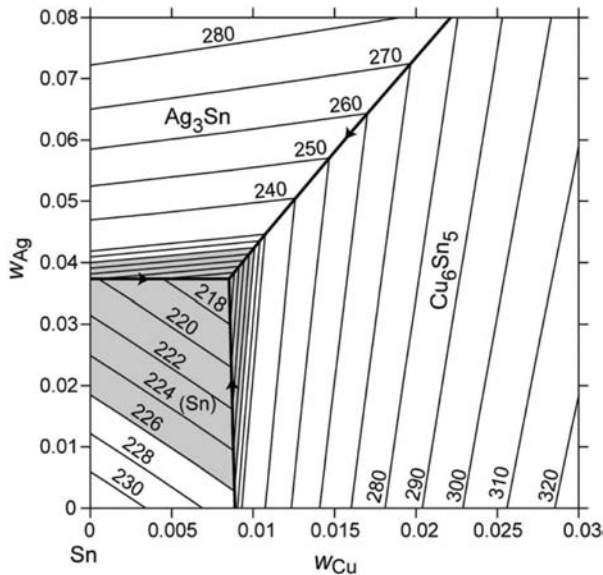


Fig. 2.11. Sn-Ag-Cu phase diagram – liquidus projection. [27]

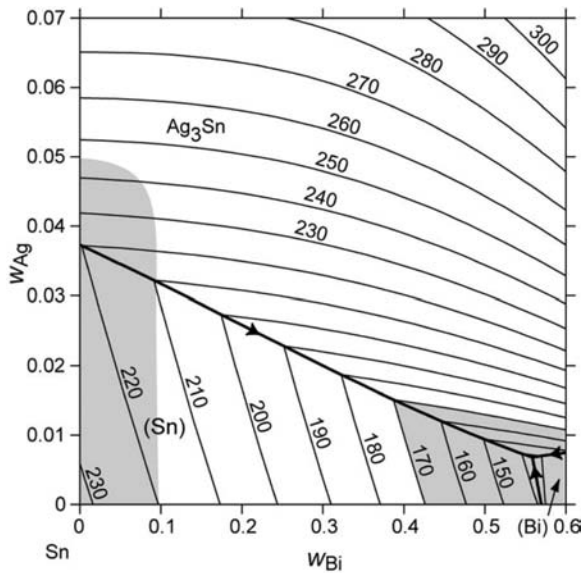


Fig. 2.12. Sn-Ag-Bi phase diagram – liquidus projection. [28]

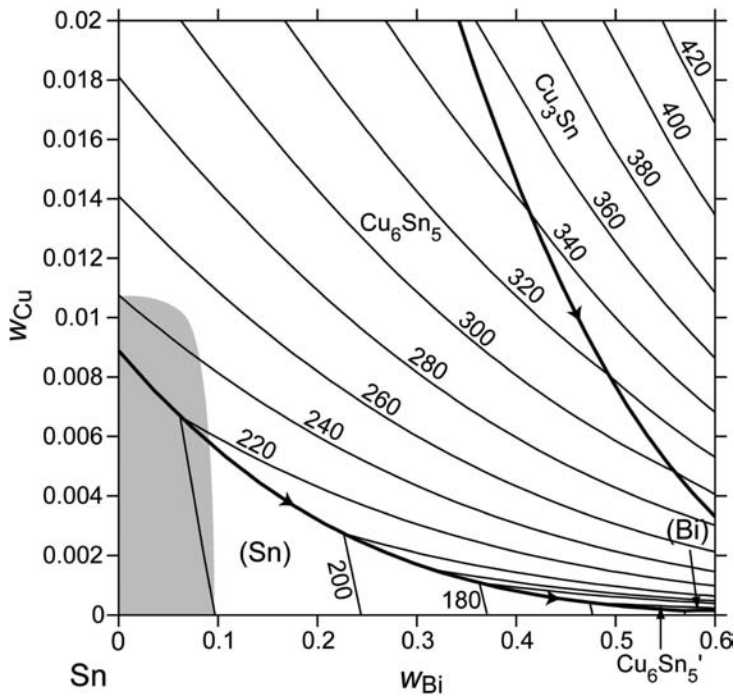


Fig. 2.13. Sn-Bi-Cu phase diagram – liquidus projection.

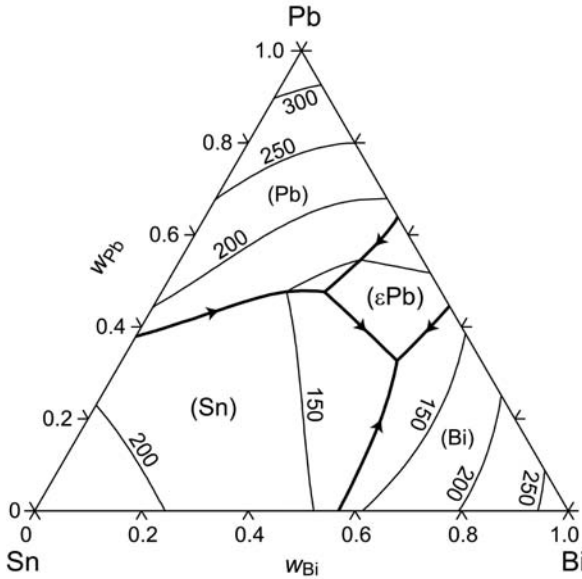


Fig. 2.14. Sn-Bi-Pb phase diagram – liquidus projection.

The NCMS Pb-Free Project member companies selected solders with liquidus temperatures less than 225°C and with an equilibrium pasty range (the difference between liquidus and solidus temperatures) less than 30°C. In the later IDEALS [11-14] and NEMI projects[15-18], candidate Pb-free solders were limited to eutectic and near eutectic, Sn-rich solders with smaller pasty ranges. Bismuth-containing solder alloys were eliminated as candidates for the primary replacement for the Sn-Pb eutectic alloy because of the possibility of forming the low temperature ternary eutectic at 96°C when a Bi-containing solder alloy is mixed with Sn-Pb surface finishes (Figure 2.14).

In the NCMS Project, it was shown that the composition dependence of the liquidus temperature for Sn-rich solder alloys could be estimated from a simple linear equation for additions of Ag, Bi, Cu, Ga, In, Pb, Sb, and Zn to Sn. [1] For Ag, Bi, Cu, and Pb, the coefficients were derived from the slopes of the Sn-X (X = Ag, Bi, Cu, Pb) binary phase diagram liquidus curves

$$T_{\ell} = 232^{\circ}\text{C} - 3.1 \cdot W_{\text{Ag}} - 1.6 \cdot W_{\text{Bi}} - 7.9 \cdot W_{\text{Cu}} - 3.5 \cdot W_{\text{Ga}} - 1.9 \cdot W_{\text{In}} - 1.3 \cdot W_{\text{Pb}} + 2.7 \cdot W_{\text{Sb}} - 5.5 \cdot W_{\text{Zn}} \quad (2.1)$$

where the coefficients are in units of $^{\circ}\text{C}$, and W_X is the amount of element X in wt.%. This equation is valid for the following alloy additions to Sn (expressed in wt.%): Ag < 3.5, Bi < 43, Cu < 0.7, Ga < 20, In < 25, Pb < 38, Sb < 6.7, and Zn < 6.

Using this equation, the maximum decrease from the melting point of pure Sn with additions of Ag and Cu was estimated to be $15\text{--}16^{\circ}\text{C}$, in agreement with the measured ternary eutectic temperature in the Sn-Ag-Cu system of 217°C , as seen in Figure 2.11. [27] From this simple equation, many alloy compositions with Bi, In, and Zn additions can be identified that exhibit liquidus temperatures of 183°C , the eutectic temperature of Sn-Pb eutectic solder. The problem with most of these alloys is that their solidus temperatures are significantly lower than 183°C . For example, the Sn-Bi binary alloy with a liquidus temperature of 183°C has a solidus temperature of 139°C . The issue of limiting the pasty range is particularly serious for through-hole wave joints, for which alloys with a large pasty range may exhibit fillet lifting as discussed further in this chapter.

One alloy that generated considerable interest was Sn-8Zn-3Bi with a liquidus temperature of 199°C and a pasty range of 10°C , thus having a significantly lower liquidus temperature than alloys in the Sn-Ag-Cu system. However, zinc-containing alloys have been observed to oxidize easily, showing severe drossing in wave solder pots, are prone to corrosion, and have a solder paste shelf life that is measured in terms of days or weeks compared to months for eutectic Sn-Pb. The bismuth is added to improve the wettability, reduce the liquidus temperature, and reduce corrosion compared with binary Sn-Zn alloys. The presence of bismuth may also result in the formation of low melting point phases in contact with Sn-Pb coated components and boards, affecting the reliability of the assembly as in the case of Sn-58Bi. Due to these issues, the use of this Sn-Zn-Bi alloy as a general replacement for eutectic Sn-Pb has been limited. [18]

The equilibrium melting behavior of four compositions in the Sn-Ag-Cu system that have been used as replacements for Sn-Pb eutectic solders is illustrated in Figures 2.15 and 2.16; with one additional high Ag/high Cu composition shown for comparison. These four solder compositions are Sn-3.0Ag-0.5Cu, Sn-3.5Ag-0.9Cu, Sn-3.9Ag-0.6Cu, and Sn-1.0Ag-0.5Cu. Figure 2.15 shows the total solid fraction as a function of temperature during heating for these four alloys. A comparison of these SAC alloys illustrates several important points regarding the sensitivity of the melting behavior to changes in composition. All of these alloys have a high fraction of Sn in the solid phase. For near-eutectic alloys, the solid alloy is $>90\%$ solid Sn that melts very close to 217°C . The total fraction of intermetallic phases over wide composition ranges is small as illustrated for the Sn-3.9Ag-0.6Cu alloy

(Figure 2.16a), and difficult to detect using standard DTA (differential thermal analysis) measurement systems.

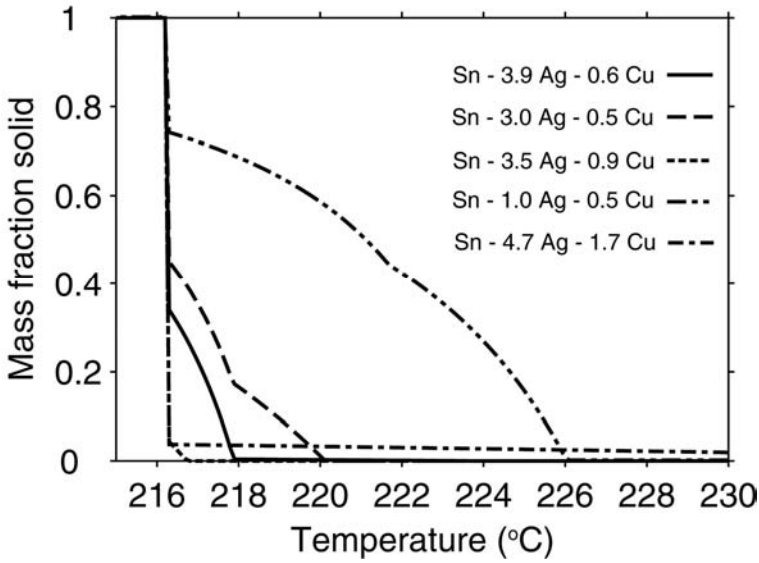


Fig. 2.15. Comparison of calculated fraction solid as a function of temperature for five different Sn-Ag-Cu alloys.

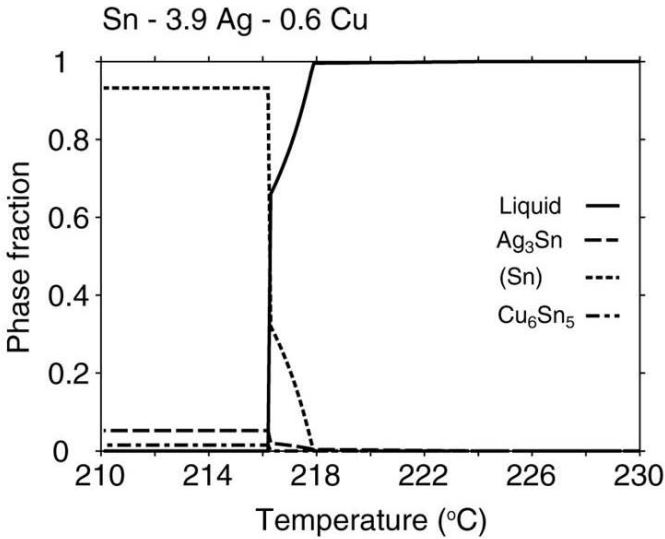


Fig. 2.16a. Calculated melting path for Sn-3.9Ag-0.6Cu.

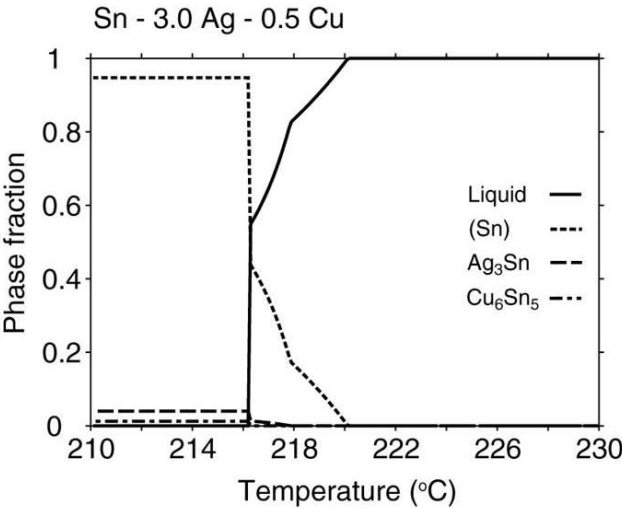


Fig. 2.16b. Calculated melting path for Sn-3.0Ag-0.5Cu.

The “effective” liquidus temperatures measured will, therefore, be 217°C for a wide range of compositions. In reflow soldering, it is likely that this small fraction of intermetallic phase will have a correspondingly small effect on solder flow and wetting, even if the solder in the joint never becomes completely liquid. For the two lower Ag alloys, the liquidus temperatures are 220°C (Sn-3.0Ag-0.5Cu) and 226°C (Sn-1.0Ag-0.5Cu). Since the fraction of Sn remaining between 217°C and the liquidus temperature is significant, the alloys must reach their liquidus temperature during assembly to properly reflow. This is illustrated in greater detail in Figure 2.16b with the equilibrium fractions of the individual phases, liquid, Sn, Ag₃Sn, and Cu₆Sn₅, shown as a function of temperature during heating for Sn-3.0Ag-0.5Cu.

Another useful representation of the melting behavior of SAC alloys as a function of temperature and composition is an isothermal section through the Sn-Ag-Cu phase diagram as presented in Figures 2.17 a-d. The experimentally determined eutectic composition of Sn-3.5(±0.2)Ag-0.9(±0.2)Cu is indicated by the black square in Figure 2.17a. When we consider the typical tolerance ranges of alloy compositions in solder pastes (±0.2), the possible melting range for the eutectic composition Sn-3.5Ag-0.9Cu becomes approximately 13°C. Likewise, when the typical tolerance of (± 0.2 wt.%) in the alloy composition is included, the NEMI alloy Sn-3.9Ag-0.6Cu, shown by the medium grey square has a possible melting range of 12°C. The third tin-silver-copper alloy Sn3.0-Ag-0.5Cu, shown by the light grey square, has a melting range of 5°C. The fourth tin-silver-copper alloy Sn-1.0Ag-0.5Cu, shown in the black framed white square, has a melting range of 11°C.

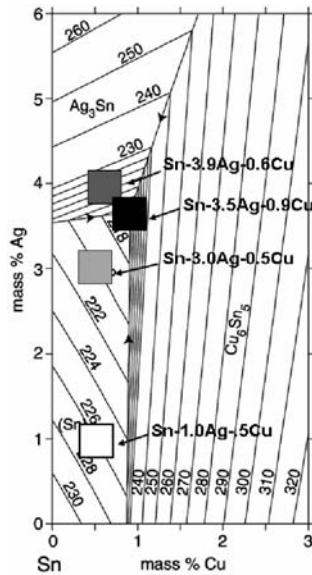


Fig. 2.17a. Liquidus projection of Sn-Ag-Cu diagram with four different alloys.

Figures 2.17b-d show the compositions over which there is <0.5% and <1% solid as the temperature is increased from 217°C, the eutectic temperature, to 219°C to 240°C to 270°C. In Figure 2.17b the region marked “L” and bounded by the black triangle is the range of compositions that are completely liquid at 219°C. The two regions outlined are compositions with less than 0.5% and 1% solid at temperatures higher than 219°C. The values of 0.5% and 1% were chosen since the presence of less than 1% solid is expected to have little or no effect on the reflow behavior of solder pastes. The remaining solid phase particles at this fraction are significantly smaller than the solder alloy powder particles from which they formed and will have a negligible effect on melting and coalescence of the alloy powders as they melt. As can be seen from Figure 2.17b, both the NEMI and the eutectic alloys have less than 1% solid remaining at 219°C. Beyond these two alloys, a wide range of alloys meet this criterion of having less than 1% solid remaining at 219°C. At 240°C (Figure 2.17c), the range of compositions with 0%, less than 0.5% and less than 1% solid remaining are extremely broad, encompassing all four alloys. [17]

The isothermal phase diagrams in Figures 2.17b-d can be used to estimate the change in solder composition of a Sn-Ag-Cu alloy held at 219°C, 240°C, or 270°C in contact with copper from the leads or pads, or silver from a

board surface finish. For examples, Figure 2.17d shows the initial alloy composition of Sn-3.9Ag-0.6Cu and the final composition, Sn-3.85Ag-1.85Cu, as determined by the solubility limit of copper in the starting alloy at 270°C. The solder alloy Sn-1.0Ag-0.5Cu is shown for comparison; the composition of the final alloy saturated with copper at 270°C is Sn-0.99Ag-1.65Cu.

Based on the analyses described, the tin-silver-copper system is quite forgiving in terms of its insensitivity of melting behavior to composition over a wide composition range. Therefore, the effect of solder composition on reflow behavior should be minimal for compositions within this range. The same holds true for wave soldering. The temperatures for wave soldering are much higher than for reflow soldering and are determined by many factors, including the activity of the flux and the board design. The initial solder alloy composition will, however, affect how much copper and other metals will dissolve in the bath, so one might conclude that the base solder should contain high amounts of copper. A tradeoff in copper concentration actually occurs: For a given silver concentration, low initial copper concentrations encourage fast dissolution from the boards and the components, while high initial copper concentrations encourage intermetallic formation in colder sections of the bath. This tradeoff has led us to suggest a copper concentration limit in the as-received solder alloy of 0.5% to 0.6% for both wave soldering and reflow of electronic assemblies.

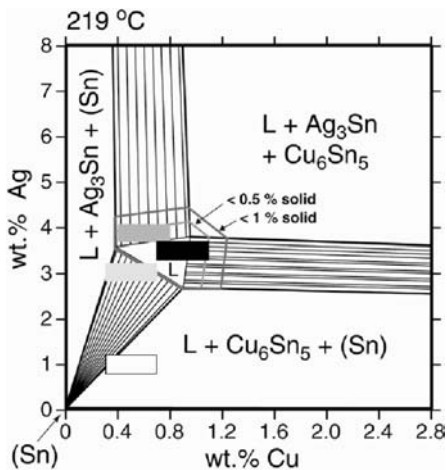


Fig. 2.17b. Isothermal section of Sn-Ag-Cu phase diagram at 219°C. Four compositions are shown with the ranges of composition allowable by industry standards corresponding to the borders of the rectangles. The region in composition space where <1% and <0.5% solid are outlined.

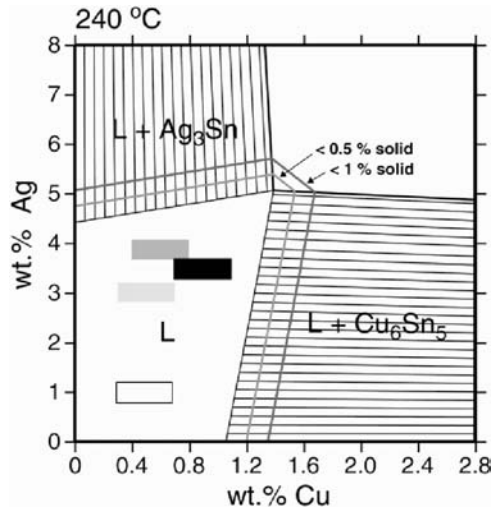


Fig. 2.17c. Isothermal section of Sn-Ag-Cu phase diagram at 240°C.

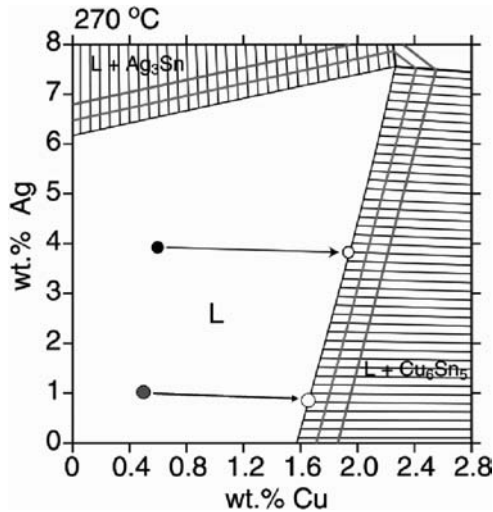


Fig. 2.17d. Isothermal section of Sn-Ag-Cu phase diagram at 270°C showing initial compositions Sn-1.0Ag-0.5Cu and Sn-3.9Ag-0.6Cu and their final compositions when they become exposed to Cu and their compositions become saturated with Cu at 270°C.

2.4.2 Copper and Nickel Dissolution into Molten Solder Alloys

The amount of copper and nickel from the substrate that dissolves into a molten solder and whether the alloy becomes saturated with respect to the substrate material are determined by the alloy thermodynamics and the dissolution kinetics. More insight into dissolution kinetics of copper in contact with SAC alloys can be found from the research of Chada et al. [30] who performed a comprehensive experimental study of the dissolution rate of Sn-3.5Ag as a function of composition and temperature for a controlled amount of solder in contact with copper. Figure 2.18 shows the effects of temperature, composition, time (t), and area of Cu-solder interface divided by the solder volume (A/V) on the dissolution of Cu in Sn 3.5Ag.

For the data presented here for the temperature range from 254°C to 302°C and for A/V values of 0.2 mm⁻¹ and 0.4 mm⁻¹, the time for complete saturation of the Sn-3.5Ag molten alloy is short, on the order of 1 minute. This situation will exist for the limited solder volumes in surface mount solder joints and within the barrels of plated-through-hole wave joints. Therefore, depending on the time, the final molten alloy compositions will be between the initial alloy composition and their corresponding Cu-saturated compositions.

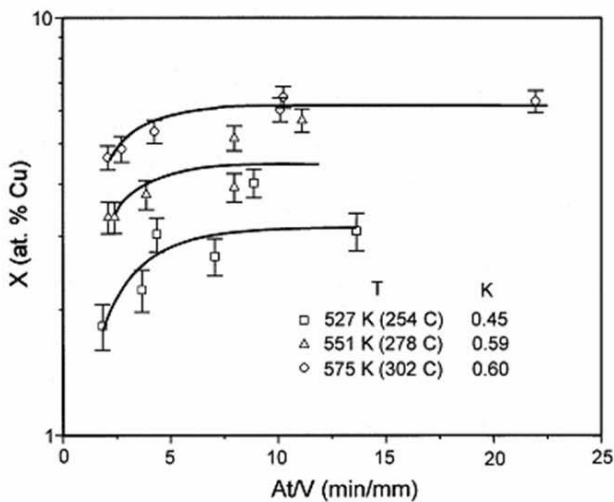


Fig. 2.18. Measurements of the average Cu content of isothermally reflowed specimens having two different substrate surface area (A) to solder volume (V) ratios and reflowed from 60 s, 120 s, 240 s. The curves represent fits of the Nernst-Brunner equation to the data. (From Chada et al. [30])

This situation is in contrast to essentially unlimited copper dissolution from the bottom-side of boards in contact with wave soldering or wave rework equipment, that is, the volume of the solder is essentially infinite compared with the area of contact between Cu and solder and the solder remains unsaturated with respect to copper.

Copper dissolution has been found to be a major factor limiting the time for wave rework of solder joints before the copper is completely dissolved. Dissolution of copper lands and barrels during rework of Pb-free plated-through hole solder joints using a wave solder process may lead to open circuits and electrical failure of printed wiring boards. Typical rework conditions for Sn-Pb eutectic solder allow for one to two rework operations using wave soldering rework equipment. The higher temperatures needed for wave rework of SAC, Sn-Ag, and Sn-Cu alloy through-hole joints lead to faster copper dissolution rates than with Sn-Pb eutectic solder. As discussed above, the Pb-free solder alloys are generally undersaturated with respect to copper and can therefore dissolve significantly more copper until they reach their solubility limits, as illustrated in Figure 2.17d for two Pb-free alloy compositions in contact with copper. Since the wave rework mini-solder fountain soldering bath used for rework has an essentially infinite volume compared to the amount of available copper that can dissolve into it, the bath will dissolve all available copper without saturation.

The presence of nickel in either a Pb-free SAC alloy or in the substrate seems to have a significant effect on the total amount of Cu, Cu-Ni or Ni substrate dissolving into the alloy and the rate at which it dissolves. Recent studies of the effect on substrate dissolution of Ni concentration in the alloy or the presence of Ni substrate instead of a Cu substrate agree with the earlier study of Korhonen et al. [31] Korhonen et al. determined that the dissolution rates of substrates with compositions between pure Cu and pure Ni into Sn-3.5Ag and Sn-3.8Ag-0.7Cu alloys depended strongly on the substrate alloy, as seen in Figures 2.19a and 2.19b. Similar results have been reported for dissolution of Cu substrates in the presence of a Ni-containing Pb-free alloy. It is thought that this effect has two primary causes: (1) the solubility limit of Ni in alloys in the Sn-Ag-Cu family is extremely low, much less than 0.1% leading to a fast local saturation of the molten alloy with alloys always close to Ni saturation and (2) the diffusion through and dissolution of the intermetallics that form on Ni, Ni-containing copper substrates, or on Cu substrates in the presence of Ni-containing solder are very slow. If the ability to rework plated-through-hole joints in wave soldering rework equipment is important, the addition of Ni to the alloy or the use of a Ni-containing substrate may provide additional flexibility in terms of rework time.

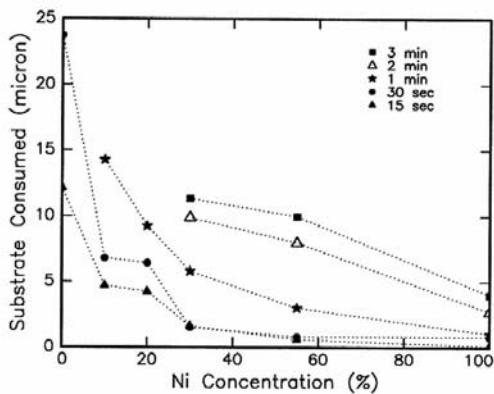


Fig. 2.19a. Substrate consumption vs. nickel content in the metal foil immersed in Sn-3.5Ag solder bath. [31]

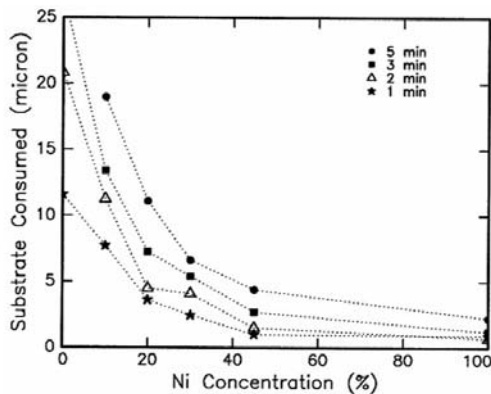


Fig. 2.19b. Substrate consumption vs. nickel content in the metal foil immersed in Sn-3.8Ag-0.7% Cu solder baths. [31]

2.5 Solidification Behavior

At first glance, it might seem reasonable to consider solidification during cooling from the liquid state as simply a reversal of the melting process, with the equilibrium solid phases forming at the equilibrium transformation temperatures. This is not the case for Sn-based alloys. There are five effects that we describe here that affect microstructural evolution: (1) difficulty of β -Sn nucleation, (2) dissolution of copper in the alloy changing the

composition of the solidifying alloy; (3) precipitation of Cu-Sn intermetallics on the Cu-Sn interface during solidification; (4) non-equilibrium solids and liquids forming due to the Scheil effect, and (5) difficulty of liquid redistribution leading to fillet lifting. A recent review by Swenson [32] discussed in detail the various transformations and microstructural features that result from solidification of SAC alloys under a wide range of conditions. This section will be followed by a discussion of the effects of these phenomena on the performance and reliability of solder joints of various compositions, particularly the SAC alloys.

2.5.1 Effect of β -Tin Nucleation and Supercooling on Microstructural Evolution

It is well known that β -Sn has difficulty nucleating during cooling of solders from the process temperature. This difficulty in nucleation leads to formation of metastable phases, supercooling of the liquid phase well below where it is stable at equilibrium, and rapid formation of Sn dendrites once nucleation has occurred. These effects dominate microstructural evolution in SAC alloys since all of the SAC alloys being used as replacements for Sn-Pb are predominantly β -Sn, with small amounts of Cu_6Sn_5 and Ag_3Sn intermetallics.

During cooling from the completely molten state, the first solid phase forming in SAC alloys depends on the composition. For the composition Sn3.9Ag0.6Cu, the first phase that forms on cooling is Ag_3Sn . The next phases expected from equilibrium thermodynamics calculations are Ag_3Sn and β -Sn. If β -Sn does not nucleate, the equilibrium phase diagram in Figure 2.11 cannot be used to predict the phases forming during cooling. A metastable phase diagram, Figure 2.20, must therefore be constructed to take into account the difficulty in nucleating β -Sn and the temperature at which β -Sn nucleation finally occurs. In the metastable transformation for Sn-3.9Ag-0.6Cu, Ag_3Sn continues to form as the supercooled liquid becomes depleted in Ag. The next stable phase to form in addition to Ag_3Sn is Cu_6Sn_5 when the composition reaches the metastable liquidus “valley” (line of two-fold saturation). The supercooled liquid continues to be depleted in Ag and Cu as the two intermetallics form. For alloys that start in the Ag_3Sn phase field, this means that there are large Ag_3Sn plates that form beginning at the liquidus surface and these continue to grow from the supercooled liquid below the eutectic temperature. At some temperature below the eutectic temperature, the supercooled liquid is sufficiently supersaturated to finally nucleate β -Sn in the presence of local heterogeneous nucleation sites in the solder. At this point, β -Sn forms as dendrites from a small number of nuclei and the solder

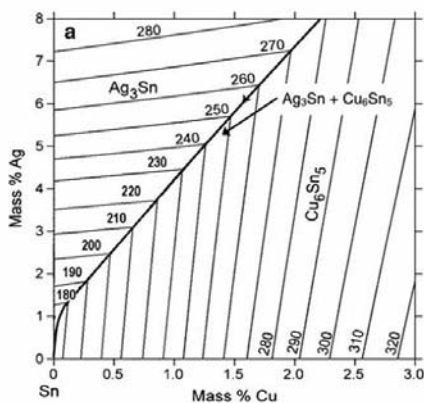


Fig. 2.20. Metastable Sn-Ag-Cu phase diagram showing no formation of β -Sn until a significantly lower temperature and with a lower Ag and copper concentration than the equilibrium ternary eutectic temperature and composition. (From Swenson, 2006 [32], recalculated using ThermoCalc)

joint solidifies completely with the remaining ternary alloy liquid forming regions with different phases and morphologies as discussed by Moon et al. [29]

The Sn-Ag-Cu phase diagram, the calculated solidification path, and DTA (Differential Thermal Analysis) results for the Sn-4.7Ag-1.7Cu are shown in Figures 2.11, 2.21a and 2.21b, respectively. At equilibrium, solidification begins with the formation of Cu_6Sn_5 at 265°C, at 238°C formation of Ag_3Sn begins and the remaining liquid should transform to a mixture of Sn, Ag_3Sn and Cu_6Sn_5 at the ternary eutectic of 217.5°C. However, in DTA experiments showing heat evolution during cooling (Figure 2.21b) from the liquid state, the first phases to form are Ag_3Sn and Cu_6Sn_5 at 244°C. Since β -Sn is difficult to nucleate, the liquid supercools by approximately 20°C while Ag_3Sn and Cu_6Sn_5 continue to form until the remaining liquid solidifies at 198.5°C. The latent heat (or heat of fusion) is released, leading to the solder self-heating to 217°C, the eutectic temperature. This phenomenon is known as recalescence. Supercooling can also be exhibited in the Sn-Pb system, but typically with a supercooling of 5°C.

This supercooling occurs even though large intermetallic particles are present which indicates that the intermetallics are ineffective as heterogeneous nucleation sites for β -Sn. As a result of the supercooling and the consequent rapid dendritic growth of β -Sn, the microstructure between the large intermetallic particles can be considered as practically an independent solidification process, forming the microstructure from an alloy with a composition much more Sn-rich than the original alloy. An analysis of the amount of supercooling (i.e., the temperature when β -Sn finally nucleates) and the slopes of the

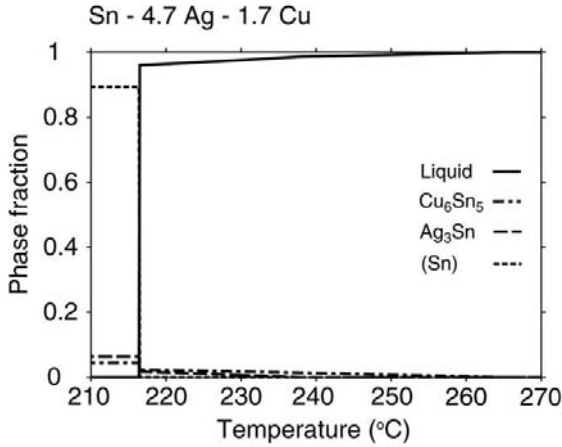


Fig. 2.21a. Calculated solidification path for Sn-4.7Ag-1.7Cu.

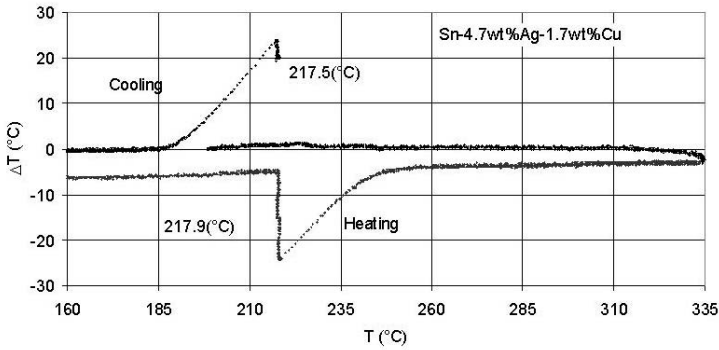


Fig. 2.21b. DTA heating and cooling curves for Sn-4.7Ag-1.7Cu. [27]

metastable liquidus surfaces allows the liquid composition at the start of growth of β -Sn dendrites to be estimated. Figure 2.22 show various microstructures between β -Sn dendrites. Moon et al. determined that solidification sequences from a wide range of SAC alloys agree with that predicted for supercooling and solidification of a more Sn-rich composition existing at the time of Sn nucleation than that expected from equilibrium processes. [27]

The metallographic sections do not reveal these solidification paths in a straightforward manner. The primary Ag_3Sn phase can be recognized as

elongated plates, usually seen edge-on. The plate morphology can be seen clearly in the etched structures from Jang and Frear [33] (Figure 2.23) and microstructures from the JCAA-JGPP study (34) (Figure 2.24). The Cu_6Sn_5 phase appears as more blocky particles in two dimensions which can be sections through rods or more equiaxed particles. The solidification sequences for the individual microstructural regions are not always apparent because of the initial difficulty in nucleating β -Sn and the subsequent rapid β -Sn dendrite growth once nucleation occurs.

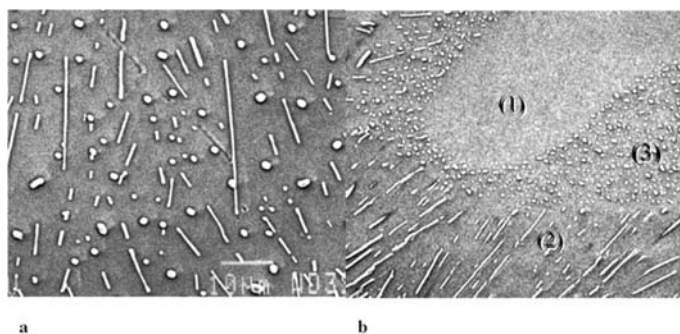


Fig. 2.22. SEM micrographs of eutectic structures: (A) ternary eutectic structure (matrix: (Sn), needle shape: Ag_3Sn , and disk shape: Cu_6Sn_5). (B) region with co-existing (Sn)+ Cu_6Sn_5 and (Sn)+ Ag_3Sn fine two phase regions near a (Sn) dendrite arm. Region labels 1 - (Sn); 2 - (Sn) + Ag_3Sn ; 3 - (Sn) + Cu_6Sn_5 ; 4 - (Sn) + Ag_3Sn + Cu_6Sn_5 . [27]

The best microstructural feature to separate the stages of solidification is the size of the largest intermetallic particles in various regions. An additional parameter that affects the phases that nucleate, their microstructures, and their resulting properties is the cooling rate, as demonstrated by Kim et al. [35] and Henderson et al. [36] Since cooling rate is not something that can be controlled in a practical way for complex assemblies, there are several other strategies that have been proposed to influence Sn-based alloys. Henderson et al. demonstrated that the formation of Ag_3Sn could be reduced and even suppressed by starting with a composition that is substantially lower in Ag than many common commercial alloys [36]. By using a typically observed supercooling of 20°C , Henderson et al. estimated that a SAC alloy must contain less than 2.7 wt% Ag to avoid formation of Ag_3Sn intermetallic plates. The intent to suppress Ag_3Sn formation before β -Sn forms has been the primary reason that the Sn-1.0Ag-0.5Cu SAC alloy has been proposed as an additional option to the higher silver compositions.

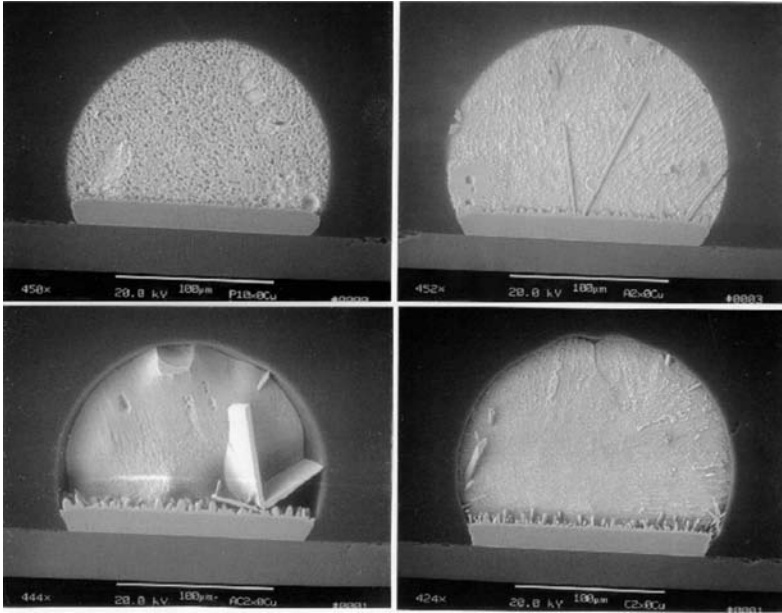


Fig. 2.23. Etched microstructures of Sn-3.5Ag showing Ag₃Sn platelets from unpublished research of Jang and Frear. [33]

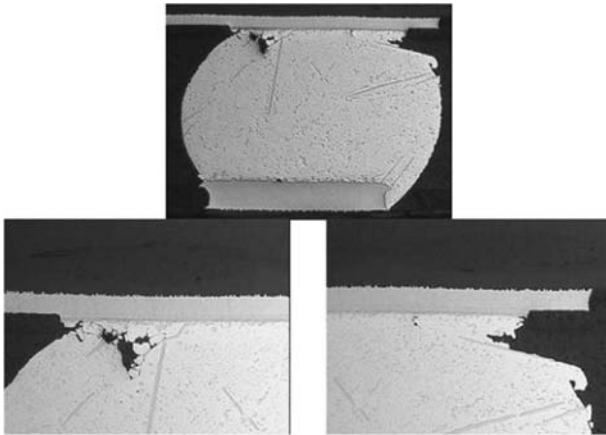


Fig. 2.24. Non-eutectic solidification behavior of Sn-Ag-Cu alloy can produce non-spherical solder ball shapes. These solder joints had very good reliabilities in thermal cycling under conditions from -55°C to $+125^{\circ}\text{C}$. From the JCAA/JG-PP study. [34]

Another strategy to avoid Ag_3Sn plate formation and promote $\beta\text{-Sn}$ nucleation has been to “inoculate” the SAC alloy with minor additions that promote nucleation of $\beta\text{-Sn}$ at temperatures and compositions closer to their equilibrium values. [37-39] Swenson presents a critical analysis of the effects of Zn-additions on melting and solidification of Sn, Sn-Ag alloys, and SAC alloys. [32] More recent research by Anderson, Syed, and Dudek [40] suggest that other additives may also be effective at forming heterogeneous nucleation sites for $\beta\text{-Sn}$.

In any discussion of the role of Ag_3Sn plate formation on thermomechanical fatigue, it should be remembered that the presence of Ag_3Sn plates does not appear to have a direct influence on either failure path or solder joint lifetime [34, 36].

2.5.2 Role of Copper Substrate Dissolution on Alloy Solidification and Intermetallic Formation

An additional complication in analyzing the microstructure is the role of the board pad-solder and component pad-solder interfaces in both shifting the solder composition from the initial composition and being a preferred site for intermetallic formation. As noted in the previous discussion on melting, the solder composition can be shifted as a result of dissolution of substrate material in the molten solder. The amount and types of intermetallic that then form during solidification will be determined by the starting composition of the alloy and how much copper and other metals from the board and component have dissolved into the molten solder. For example, for the composition Sn-3.9Ag-0.6Cu at 270°C noted in Figure 2.17d, dissolution of copper in the solder joint can bring the overall composition to Sn-3.85Ag-1.85Cu when the liquid solder has dissolved the maximum amount of copper it can.

The formation of large Ag_3Sn plates depends on the composition in the joint being in the Ag_3Sn primary phase field. If, as a result of copper dissolution in the molten solder alloy, the copper concentration becomes high enough in the solder joint for the primary phase to be Cu_6Sn_5 rather than Ag_3Sn , then Cu_6Sn_5 will be the first phase that forms from the molten solder during cooling and not Ag_3Sn as in the original alloy composition. As the solder joint cools, Cu_6Sn_5 intermetallics form in the solder joint, both at the pre-existing intermetallics at the interfaces between the solder and the board and component metallizations and as rods in the solder itself.

2.5.3 Non-Equilibrium Effects of Diffusion in the Solid on Equilibrium Solidification

The pasty ranges based on equilibrium phase diagrams and the Lever Rule are the minimum pasty ranges that can occur during solidification. Segregation in the solid during solidification and metastable phase formation may extend these ranges in solder systems that exhibit substantial changes in the solubility of solid Sn during cooling. The amount of liquid present during cooling can be greater than predicted from the equilibrium phase diagram as a result of the well-known Scheil effect. In Lever Rule calculations, complete mixing in the liquid and complete diffusion in the solid at each temperature are assumed to have occurred during cooling to create the conditions of equilibrium. In Scheil calculations, complete mixing in the liquid is assumed but no diffusion in the solid is allowed during cooling. This leads to conditions only of local equilibrium at the solid-liquid interface during solidification, but not to equilibrium of the system.

Tin-based solder systems that exhibit this effect are Sn-based alloys containing bismuth, indium, and lead. For example, as a Sn-10Bi solder alloy is cooled from its liquidus temperature, the first solid that forms is Sn containing significantly less Bi than the Sn (Bi) solid solution at the eutectic temperature. If there is sufficient solid-state diffusion to maintain the equilibrium solid composition as the alloy cools, the final liquid transforms to a uniform solid solution at approximately 190°C, the equilibrium temperature and composition. If diffusion in the solid does not establish the equilibrium solid composition at each temperature as the alloy cools, the remaining liquid becomes increasingly Bi-rich, and has been observed to solidify at the eutectic temperature. For a Sn-6Bi solder, the liquidus temperature is approximately 224°C and the equilibrium pasty range is approximately 26°C; in the limit of no diffusion in the solid, the pasty range can be as large as 85°C. In the NCMS Pb-free Solder Project, DTA measurements of Sn-6Bi detected a measurable fraction of eutectic liquid that solidified at 139°C and, therefore, the non-equilibrium pasty range of 85°C as predicted by Scheil calculations [1-4].

The difference between the Scheil and Lever calculations is illustrated in Figures 2.25a and 2.25b for the ternary Sn-Ag-Bi system with calculations of the solid fraction as a function of temperature and composition. [Ref. 1-4] The liquidus projection of the ternary phase diagram is shown in Figure 2.12, where the lines correspond to compositions with the same liquidus

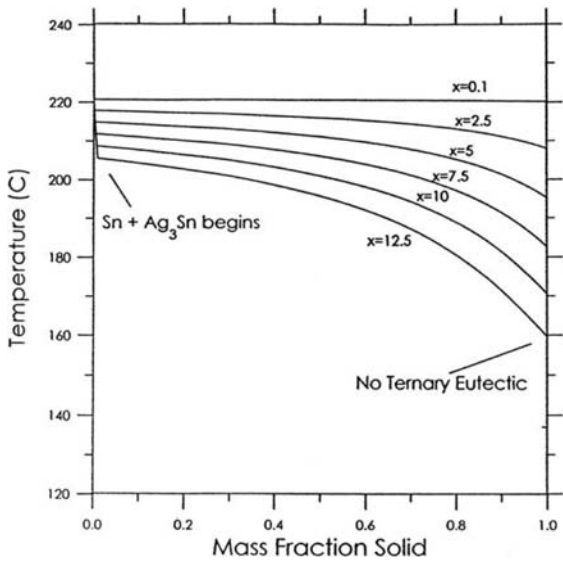


Fig. 2.25a. Lever solidification calculation for Sn-Ag-Bi. [1]

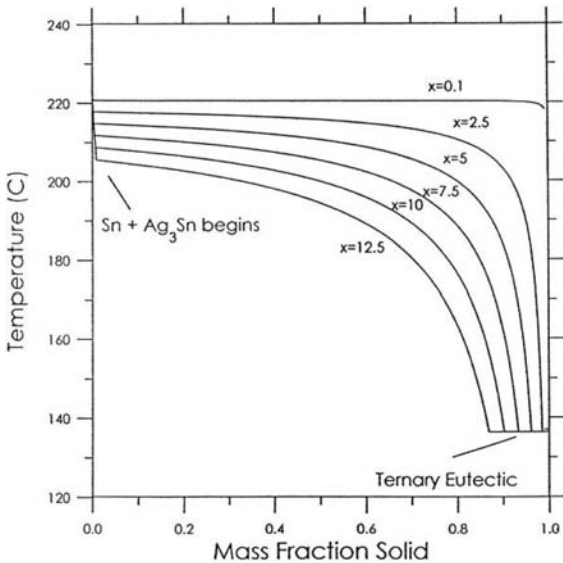


Fig. 2.25b. Scheil solidification calculation for Sn-Ag-Bi. [1]

temperatures. Considering the composition Sn-3.5Ag-7.5Bi, the last liquid solidifies at 185°C based on the equilibrium phase diagram; however, as a result of segregation during solidification, some liquid is predicted to still be present until the ternary eutectic temperature of 138°C. The amount of non-equilibrium liquid present depends on the cooling conditions and will be between the limits defined by the two curves for Sn-3.5Ag-7.5Bi in Figures 2.25a and 2.25b. In systems like Sn-Ag-Cu, there is little solubility of Ag and Cu in Sn and non-equilibrium solidification due to interdiffusion in the solid and the Scheil effect play a minor role in the behavior of SAC alloys.

2.5.4 Fillet Lifting

Fillet lifting is a defect-formation phenomenon for wave soldered through-hole joints that occurs during solidification for some Pb-free solders that does not typically occur for eutectic Sn-Pb. Fillet lifting, as shown in the micrograph in Figure 2.26, is characterized by the complete or partial separation of a solder joint fillet from the intermetallic compound on the land near the shoulder of the through hole. This phenomenon was first identified in 1993 by Vincent and co-workers [8-10] in the UK DTI (Department of Trade and Industry)-sponsored Pb-free solder project. [8] In that study fillet lifting was attributed to the presence of the Sn-Bi-Pb ternary eutectic (98°C) resulting

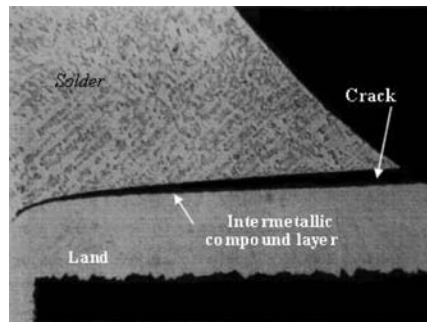


Fig. 2.26. Optical microscope cross section of fillet lifting in a through hole solder joint with Sn-3.5Ag-5Bi alloy. [1]

from Pb contamination of Bi-containing solders from the Sn-Pb hot-air-solder-leveled (HASL) board finish. While this can create the conditions for fillet lifting, this effect is now known to occur without Pb contamination for many Pb-free solder alloys, particularly for alloys containing Bi.

Suganuma, Boettinger et al. and Takao and Hasegawa have determined that fillet lifting is the result of “hot tearing,” a mechanism that leads to the relief of thermally induced stresses *when the solder is between 90% and 100% solid*. [41-43] The differential shrinkage due to CTE mismatch between the board and the solder generates stresses in the circuit board and the solder as the solder solidifies. At lower solid fractions during solidification, fluid flow occurs relieving the stresses. As the volume fraction of liquid decreases, the stresses are carried by the dendritic matrix and failures occur at the weakest point, typically the location with the highest remaining liquid fraction: the board-side intermetallic compound/solder interface. The tendency for fillet lifting increases as the pasty range increases and the temperature difference between 90% and 100% solid ($\Delta T_{90\% \rightarrow 100\%}$) increases. It is typically worse for alloys with a large non-equilibrium pasty range, like Sn-Bi or Sn-Ag-Bi. Takao and Hasegawa[43] have quantified the tendency to fillet lifting as a function of alloy composition in terms of the enthalpy (energy) change as a function of composition and temperature during cooling which corresponds directly to $\Delta T_{90\% \rightarrow 100\%}$.

In the NCMS Pb-free solder project, “hot tearing” as the origin of fillet lifting was tested by taking Sn-3.5Ag, an alloy that showed minimal fillet lifting, and transforming it into an alloy showing close to 100% cracked joints with the addition of 2.5 wt% Pb. [1] The addition of 2.5% Pb increased the pasty range from 0°C to 34°C. The NCMS study predicted that Pb contamination from Sn-Pb surface finishes would lead to fillet lifting in alloys that in their uncontaminated state showed little or no fillet lifting. Subsequent large-scale industrial wave soldering trials revealed fillet lifting in through-hole joints with Sn-Ag, Sn-Cu, or Sn-Ag-Cu solders when combined with Sn-Pb surface finished components and/or boards. [44-45] It should also be remembered that Sn-Ag, Sn-Cu, and Sn-Ag-Cu fillets may also show fillet lifting for very thick boards without Pb contamination, as indicated in the NCMS Pb-Free Solder Project. [1] Fillet lifting under these conditions is a result of the supercooling, dendritic growth, and recalescence behavior described previously. Fillet lifting appears to be a cosmetic effect only: there have been no reported solder joint failures attributed to fillet lifting.

2.5.5 Solidification and Surface Porosity

As discussed above, solidification of high-Sn Pb-free alloys occurs with the formation of Sn dendrites as seen in the as-solidified structure in Figure 2.27a. The formation of Sn dendrites is accompanied by the redistribution of the interdendritic liquid and, ultimately, by a retraction of the remaining liquid as it redistributes and solidifies. The volume of the liquid is larger than the volume of the solid; solidification, therefore, leads to shrinkage and formation of porosity. This retraction of the interdendritic liquid leads to a rough outer surface in Figure 2.27a and, correspondingly, to an overall greater surface roughness than Pb-Sn eutectic, as seen in the SEM micrograph in Figure 2.27b. These micrographs indicate why the surfaces of properly soldered Pb-free solder joints appear significantly rougher than equally well-soldered Pb-Sn solder joints and with the visual inspection criteria for Pb-free solder joints discussed in the industry standard document IPC-A-610D (Acceptability of Electronic Assemblies) to indicate that a duller, rougher appearance for lead-free solder joints is not grounds for rejection. The dendritic microstructure causing the roughness is an intrinsic characteristic of the Pb-free alloys. The scale of the surface roughness depends

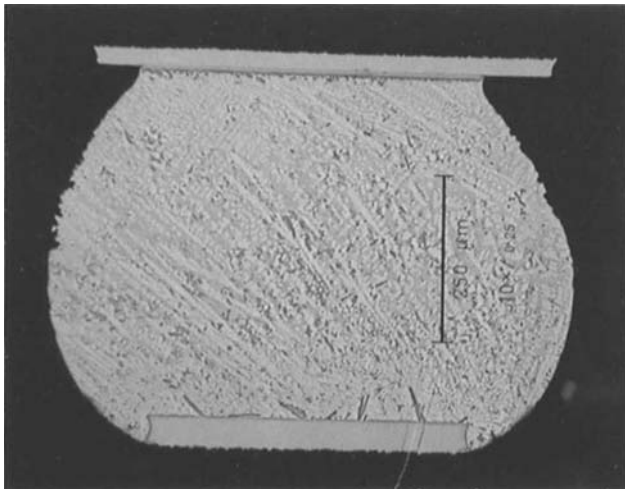


Fig. 2.27a. Cross section showing surface roughness of Sn-Ag-Cu alloy as solidified. [18]

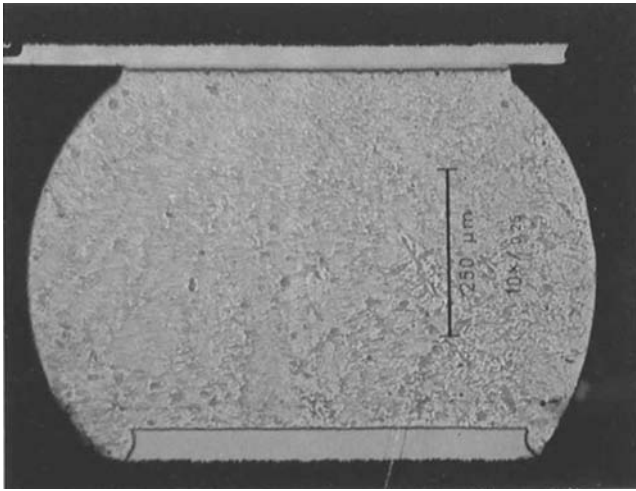


Fig. 2.27b. Cross section showing smooth surfaces of Sn-Pb alloy as solidified. [18]

on several factors, including the final joint composition and the cooling rate of the joint. The IDEALS project examined the effect of these surface “pores” caused by retraction of the solidifying interdendritic liquid on where the solder joint fails during thermal cycling. They determined that the surface “pores” between the dendrites were not preferential sites for solder joint failure. [14] Failure analysis of solder joints from a wide variety of components on thermally cycled assemblies in the NEMI Lead-Free Assembly Project did not show an effect of surface porosity on failure path or crack nucleation. [18] Hillman and his colleagues in the JCAA/JG-PP No-Lead Solder Project Report on thermal cycle testing also reported that there was no effect of porosity or position of Ag_3Sn plates on thermal cycle reliability, even for the extreme microstructures shown in Figure 2.24. [34]

2.5.6 Contamination of Pb-Free Solders

The use of a solder-coated board or component surface finish with a different composition than the solder paste or wave soldering alloy may result in different properties of the solder joints than expected from solder joints

made from the paste or wave composition alloy alone. For Pb-contamination in particular, the liquidus temperature decreases by 1.3°C (per mass fraction $\text{Pb} \times 100$), which can be calculated using Equation 2.1. The next question to be answered is how the Pb contamination affects the solidus temperature, the lowest temperature where liquid exists. When Pb-free solder alloys are contaminated by Pb from the pre-tinned layer, the last liquid that solidifies may form a low melting eutectic. This case was studied in detail for Pb-contaminated Sn-Bi solders by Moon et al. using DTA methods in conjunction with calculations of the equilibrium phase diagram and Scheil solidification. [29] They found that contamination of Sn-Bi eutectic, Sn-5Bi, and Sn-10Bi alloys by 6% Pb results in the resulting alloy following the Scheil solidification path for liquid and solid and, hence, a measurable fraction of low melting Sn-Bi-Pb eutectic forms in these alloys at 95°C because the resulting alloys follow the Scheil path during solidification. In contrast, a similar study on the effect of Bi contamination on solidification of Sn-Pb solder alloys found introduction of small amounts of Sn-Bi from component surface finishes into Sn-Pb eutectic solder paste result in alloys following more closely the Lever Rule path. [46] The solidus and liquidus temperatures are slightly lower than those of the uncontaminated solders but there is no discernable amount of low melting point Sn-Pb-Bi ternary eutectic.

Since the freezing ranges of other Pb-free solder alloys may be similarly susceptible to Pb contamination, the freezing behavior of four additional solder alloys was studied by Kattner and Handwerker using Lever rule and Scheil freezing path calculations of the original solder alloy and the contaminated solder. [26] The level of contamination was chosen to be 6% Pb from the Moon et al. estimate of a Pb-concentration of 6% (mass fraction) in the solder from contamination by the component lead and board pre-tinning. [29] The original solder compositions and those resulting from Pb-contamination are listed in Table 2.3.

Table 2.3. Modified solder compositions as a result from contamination with 16% of 63% Sn-37% Pb solder. (Compositions are in % of mass fraction)

Original Solder Composition	Contaminated Solder Composition
Sn - 3.5% Ag	Sn - 2.9% Ag - 6% Pb
Sn - 4% Ag - 1% Cu	Sn - 3.4% Ag - 0.8% Cu - 6% Pb
Sn - 3.5% Ag - 4.8% Bi	Sn - 2.9% Ag - 4% Bi - 6% Pb
Sn - 3.4% Ag - 1% Cu - 3.3 % Bi	Sn - 2.8% Ag - 0.8% Cu - 2.8% Bi - 6% Pb

The calculations were carried out using the NIST solder database [47], the Thermo-Calc software package [48] and the Scheil and Lever programs [49]. Figures 2.28a-b show the calculated fraction solid as a function of temperature for Sn-3.5Ag and Sn-4Ag-1Cu and for the corresponding alloys contaminated by 6% Pb. Contamination of the binary eutectic alloy Sn-3.5Ag with 6% Pb lowers the liquidus temperature from 221°C to 213°C and lowers the solidus from 221°C to 177°C, creating an alloy with an equilibrium pasty range of 44°C. Likewise, Pb contamination of Sn-4Ag-1Cu alloy leads to a 2°C increase in the liquidus temperature from 225°C to 227°C and a decrease in solidus temperature from 215°C to 177°C.

2.6 Wetting and Solderability

Wetting of a liquid on a solid is determined by the relative energies of the liquid-vapor surface tension, the solid-liquid interfacial energy, and the solid-vapor interfacial energy, as represented by Young’s Equation. The thermodynamics of an alloy play a central role in determining its intrinsic liquid-vapor surface tension. It is well known that the surface tension of pure Sn is significantly higher than Sn-Pb eutectic, as measured by White

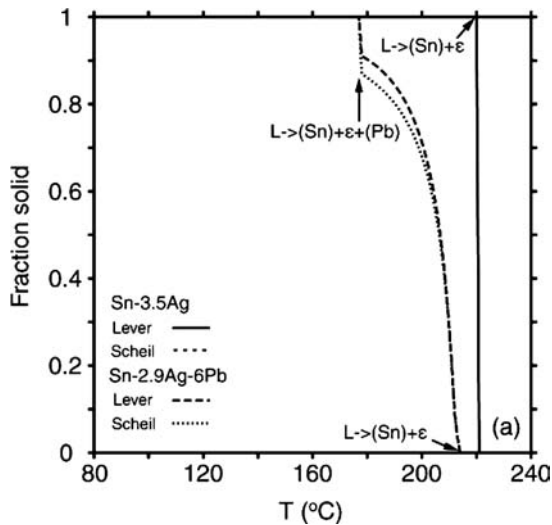


Fig. 2.28a. Lever and Scheil calculations for fraction solid as a function of temperature for Pb-free solders without and with 6% Pb contamination for Sn-3.5Ag. [26]

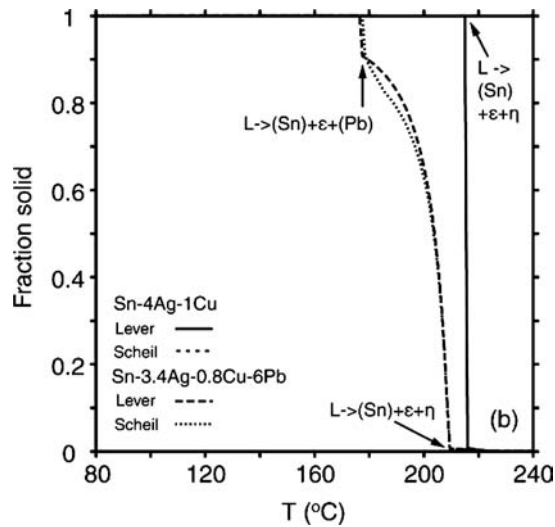


Fig. 2.28b. Lever and Scheil calculations for fraction solid as a function of temperature for Pb-free solders without and with 6% Pb contamination for Sn-4Ag-1Cu. [26]

as a function of temperature from pure Sn to pure Pb. [50] Ohnuma and his colleagues have used thermodynamic parameters to predict the surface tension and viscosity of the Sn-based liquids as a function of composition. [51-52] The higher surface tension of Pb-free high tin alloys over Sn-Pb alloys translates into generally higher contact angles for Pb-free alloys, less bridging between component leads, and a smaller process window for Pb-free solders than for Sn-Pb eutectic.

Evaluation of solderability in manufacturing has considerably greater complexity than wetting of an unreactive liquid on a substrate in a controlled laboratory environment as assumed by Young's equation [53]. Simple wetting balance and area-of-spread measurements are useful for separating the effects of solderability factors, such as flux, temperature, and substrate conditions, and for screening materials and soldering conditions when comparing different solder alloys. Manufacturing issues are discussed in detail in Reflow, Wave and Rework Chapters of this book. Through numerous national and international Pb-free solder R&D projects using wetting balance measurements, solderability was found to be a major issue in discriminating between solder alloys only for Zn-containing alloys, and then only for concentrations greater than 1% Zn. [1]

For Pb-free alloys not containing Zn, their wetting characteristics on a specific metal substrate depend on the composition of the solder and the substrate, the temperature of the solder and the substrate, the size and thermal conductivity of the substrate, the liquidus temperature of the solder, the surface condition of the substrate, the gaseous experimental environment (oxygen, air, nitrogen), and, last but not least, the flux. A comparison of wetting balance data for various Pb-free solder alloys on copper from the IDEALS and NCMS projects indicates that: (1) in general, the temperature for similar wetting balance performance to eutectic Sn-Pb scales with the liquidus temperature of the Pb-free solder, and (2) the effect of the variables listed above are separable. Figure 2.29 from the IDEALS Pb-Free Project shows that the time to 2/3 wetting force for five Pb-free solder alloys compared with Sn-40Pb at three temperatures per alloy, $T_l + 25^\circ\text{C}$, $T_l + 35^\circ\text{C}$, and $T_l + 50^\circ\text{C}$. [11-14] With the exception of Sn-0.7Cu, the character-ACTIEC 5 flux with 0.5% Cl which aids wetting (Figure 2.29a). When the flux is changed to pure Rosin flux with 0% Cl, four of the five Pb-free solders are again virtually identical to Sn-40Pb (Figure 2.29b). Only Sn-0.7 Cu-0.5Bi shows significantly poorer wetting than the other five solders.

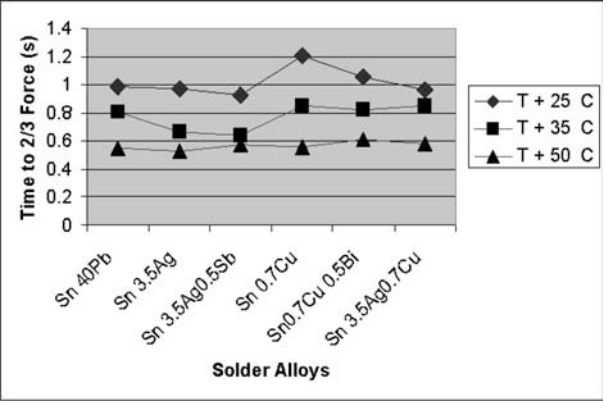


Fig. 2.29a. IDEALS project wetting data: wetting balance parameter, time to 2/3 force as a function of alloy composition for three different temperatures relative to the liquidus temperature for Actiec 5 flux. [11-14]

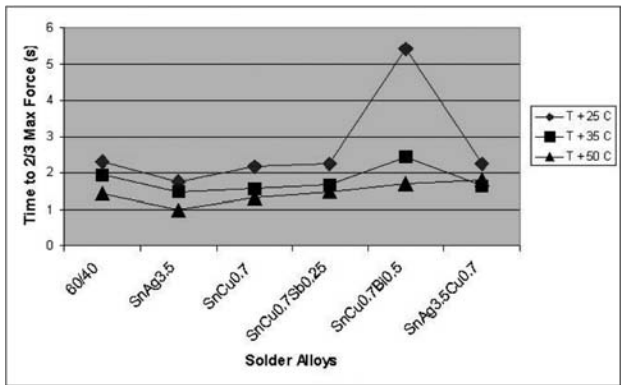


Fig. 2.29b. IDEALS project wetting data: wetting balance parameter, time to 2/3 force as a function of alloy composition for three different temperatures relative to the liquidus temperature for rosin flux. [11-14]

Bradley and Hranisavljevic have provided a thermodynamic basis for understanding the effect of alloy composition and surface finish/lead metal composition on wetting behavior based on how the liquidus temperatures change with dissolution of the surface finish or lead material into the solder. [54] They determined the temperatures at the start of solder paste coalescence and at full wetting, when all the solder particles are completely coalesced into a molten solder mass, for the alloys Sn-3.5Ag, Sn-3.8Ag-0.7Cu, Sn-1Ag-3Bi, Sn-1Ag-4.8Bi, and Sn-1Ag-7.5Bi and for four surface finishes. Figure 2.30

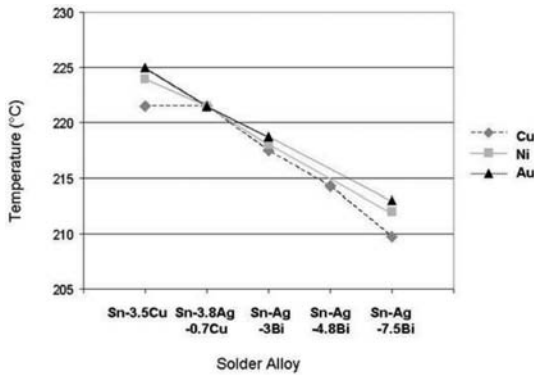


Fig. 2.30. Temperature at which solder paste begins to coalesce as a function of PCB substrate finish. Note the effect of Cu on depressing the coalescence temperature and therefore the effective wetting temperature of alloys without Cu. [54]

shows that the measured coalescence temperatures for all the solder alloy pastes, except for Sn-3.8Ag-0.7Cu, decrease with dissolution of the surface finish metal into the solder, with copper surface finish producing the greatest effect, followed by gold. This decrease in solder coalescence temperatures corresponds to a decrease in the liquidus temperatures produced by dissolution of the surface finish into the solder alloy. The alloy Sn-3.8Ag-0.7Cu is close to the ternary eutectic composition and the solidus temperature for this alloy is therefore unaffected by Cu dissolution.

2.7 Pb-Free Solder Mechanical Behavior and Solder Joint Reliability

2.7.1 Microstructure and Composition Effects on Solder Joint Mechanical Behavior and Reliability

The reliability of solder joints in assemblies is considered in more detail in the Reliability Chapter of this book. The intention of this section is to provide some physical insight into the composition and microstructural basis for the differences in mechanical and accelerated thermal cycling behavior of Pb-free alloys and Sn-Pb eutectic solder. A typical approach to estimating solder alloy and solder joint reliability is to rank alloys based on mechanical property values obtained in a particular test for a specific test condition or for a particular application. This testing can take the form of accelerated thermal cycling of a component solder joint or a simulated solder joint, creep at a particular temperature for different applied stresses or imposed strain rates, or even room temperature tensile stresses. The problem that has emerged is that the ranking of different Pb-free alloys with respect to Sn-Pb and to each other can change dramatically depending on the test condition chosen to be “representative.”

The essence of the problem has been described well and in detail by J. P. Clech for Sn-Pb as well as Pb-free solders in the following statement [55]:

“The mechanical behavior of solder depends on the joint microstructure and is affected by many parameters such as intermetallics, joint or specimen size, cooling rate of the assembly after soldering, aging in service, etc. Test factors such as specimen or load eccentricity, temperature variations and measurement errors also contribute to the scatter in the mechanical properties of solder as is well known, for example, for steady state creep.”

Alloy solder joints are composed of heterogeneous microstructures with features that vary from the tens-of-micrometers scale to the sub-100 nm

nano-scale. Eutectic Sn-Pb and near-eutectic Sn-Pb alloys are composed of a small number of eutectic colonies of lamellar Sn and Pb. Tin-based Pb-free alloys contain multiple phases that occur at multiple size scales depending on the local cooling conditions during the solidification process and on subsequent aging and deformation conditions as seen for a SAC alloy in Figure 2.22. For Sn-3.5Ag, the eutectic Sn-Ag alloy composition examined in detail by Chawla et al., cooling from above the eutectic temperature first results in the formation of Ag_3Sn plates since the high Sn-alloys do not solidify with a classic eutectic structure as a result of the difficulty in nucleating the β -Sn phase as reviewed in Section 2.4.1. [56-58] The size of the platelets depends on the cooling rate. Once the β -Sn phase is able to nucleate, β -Sn dendrites form with interdendritic Ag_3Sn of an intermediate scale and sub-100nm Ag_3Sn particles within the dendrites, with the size of all features depending on cooling rate.

Kerr and Chawla have elucidated the role, for example, of sub-100 nm Ag_3Sn precipitates on creep and grain boundary and dislocation motion in Sn-3.5Ag, as seen in Figure 2.31. [56] Figure 2.31a-c shows Ag_3Sn precipitates in β -Sn that pin the grain boundary in the as-solidified state and following deformation. Deformation produces dislocations whose motion is also pinned by the Ag_3Sn precipitates, as seen by the increased dislocation content and the intersections of dislocations and Ag_3Sn precipitates. For alloys containing Cu or Ni, either because it was in the initial alloy or

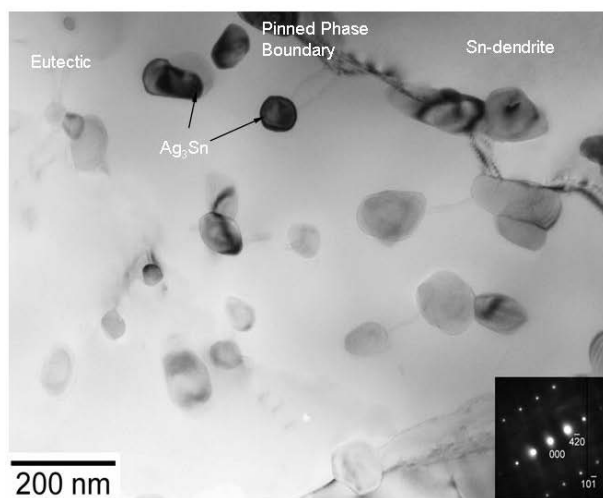


Fig. 2.31a. TEM micrographs from Kerr and Chawla showing microstructures of Sn-3.5Ag as solidified with the eutectic mixture containing the Ag_3Sn particles, Sn-dendrite, and the pinned boundary between the two phases. [56]

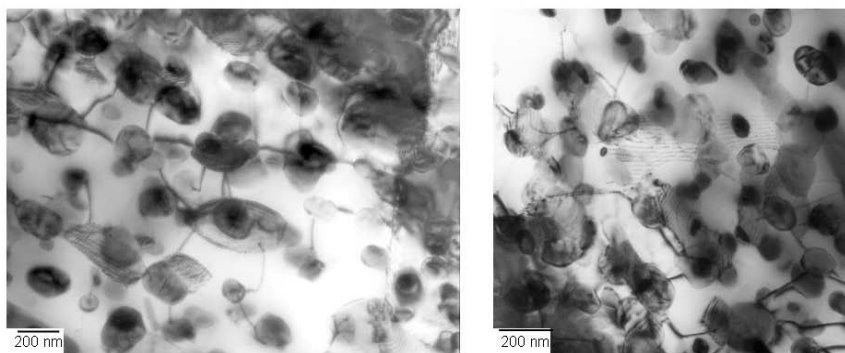


Fig. 2.31b, c. TEM micrographs from Kerr and Chawla showing microstructures of Sn-3.5Ag after creep deformation (22 MPa at 60°C, with a strain rate on the order of 10^{-4} /s, $\langle 110 \rangle$ zone axis): (b) Dislocations pinned by Ag_3Sn particles in the eutectic mixture after creep deformation (c) Pinning of dislocation substructure by Ag_3Sn particles. [56]

due to dissolution of the surface finishes, pad, and lead material into the solder, the structures will also contain additional intermetallic compounds whose size, scale and location depend on cooling rate.

Coarsening of these heterogeneous microstructures then occurs at room temperature and above for Pb-free alloys as well as for eutectic and near-eutectic Sn-Pb. [55] This leads to differences in mechanical properties for a given alloy solder joint with cooling rate, time after solidification, and thermal and stress history. [56] This contributes to the differences observed between seemingly “identical” experiments and between solder joints of the same alloy tested under different conditions.

In general, high-Sn Pb-free solders are stronger and have a higher creep resistance than Sn-Pb eutectic and near eutectic alloys. The creep data from Frear comparing the behavior of different solder alloys shown in Figure 2.32 [59] and yield strength data from the IDEALS project [11-14] as a function of composition and temperature shown in Figure 2.33 illustrate the major difference between Sn-Pb and high-Sn lead-free alloys. The dependence of the relative creep behavior of solder alloys on temperature, composition, and applied stress even in simple testing conditions is illustrated in the research of Guo et al. described in Table 2.4. [60] The differences seen here also show how changes in alloy composition resulting from reaction with the surface finishes or lead and substrate materials further change the alloy performance. Additional analyses by Guo et al. suggested that annealing the samples can have a profound effect on the creep behavior: the lower

creep resistance seen in the Darveaux data in Figure 2.34 was attributed to the pre-annealing treatment applied to the samples tested by Darveaux in contrast to the Guo samples that were tested within one week of fabrication. [60-61]

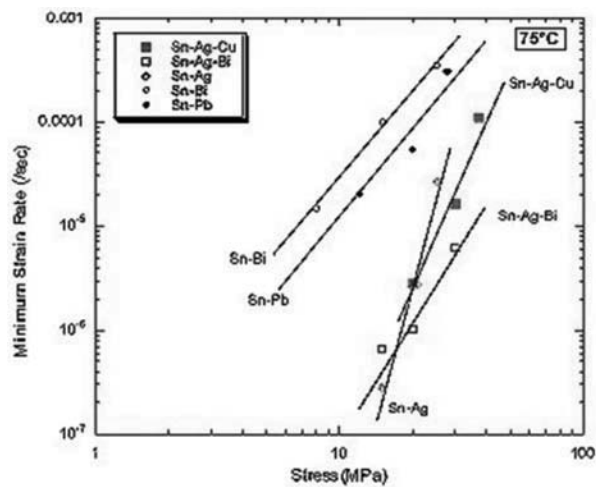


Fig. 2.32. Creep data for Sn-Pb eutectic, Sn-Bi eutectic and other compositions at 75°C as a function of applied stress. [59]

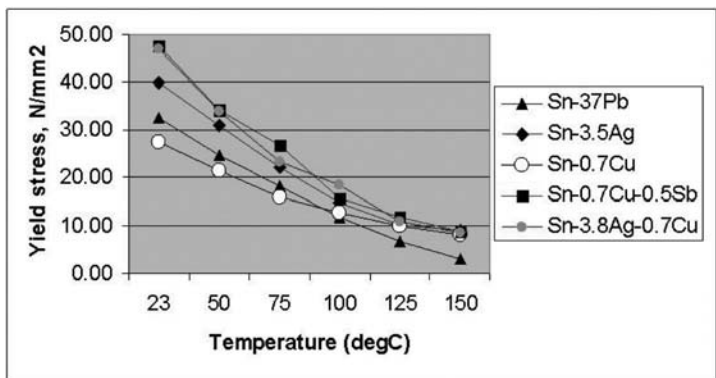


Fig. 2.33. Yield stress as a function of composition and temperature in °C. [11-14]

Table 2.4. Ranking of creep resistance of solder alloys based on best-fit power law creep by Guo et al. [60]

	Approx. 10 MPa low stress rank	Approx. 20 MPa high stress rank
Room Temperature		
Least creep resistant to	Sn-2Ag-1Cu-1Ni	Sn-4Ag-0.5Cu
	Eutectic Sn-3.5Ag	Sn-3.5Ag-0.5Ni
Most creep resistant	Sn-4Ag-0.5Cu	Sn-2Ag-1Cu-1Ni
	Sn-3.5Ag-0.5Ni	Eutectic Sn-3.5Ag
85°C		
Least creep resistant to	Sn-2Ag-1Cu-1Ni	Sn-2Ag-1Cu-1Ni
	Sn-4Ag-0.5Cu	Sn-3.5Ag-0.5Ni
Most creep resistant	Eutectic Sn-3.5Ag	Sn-4Ag-0.5Cu
	Sn-3.5Ag-0.5Ni	Eutectic Sn-3.5Ag

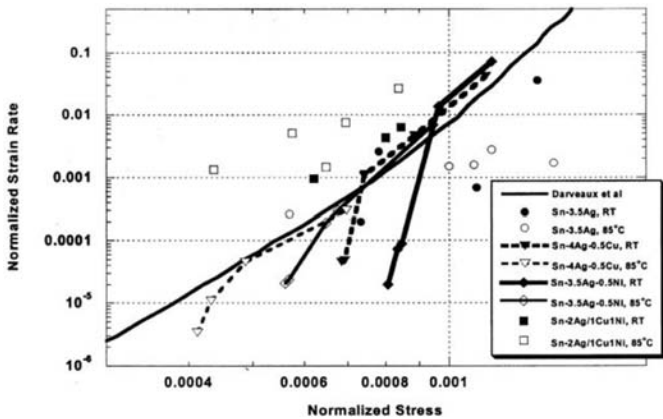


Fig. 2.34. Normalized steady-state creep strain rates versus normalized stresses for eutectic Sn-3.5Ag, Sn-4Ag-0.5Cu, Sn-2Ag-1Cu-1Ni and Sn-3.5Ag-0.5Ni solder joints along with Darveaux’s data for aged eutectic Sn-3.5Ag solder joints. From Guo et al. [60]

Similarly careful experiments, performed to determine the dominant mechanisms for deformation during thermo-mechanical fatigue or creep, have come up with opposite results regarding the dominant mechanisms. For example, on the importance of grain boundary sliding to creep in Sn-3.5Ag, particularly with respect to the role of low angle boundaries. [56, 60] These differences are likely the result of microstructural or sample history differences outlined previously. What this suggests, therefore, is that general

trends alone should be used to compare alloys: the variability in mechanical performance due to all the factors described, many times due to uncontrollable factors, leads to a large uncertainty in the performance of any solder joint.

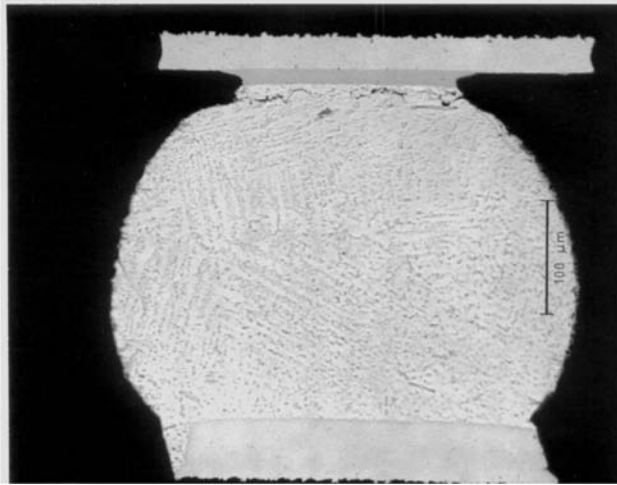


Fig. 2.35a. NEMI Lead-Free Assembly Project cross sections of 169 CSP Solder Joints fabricated with Sn-3.9Ag-0.6Cu after ATC: 0°C to 100°C. [18]

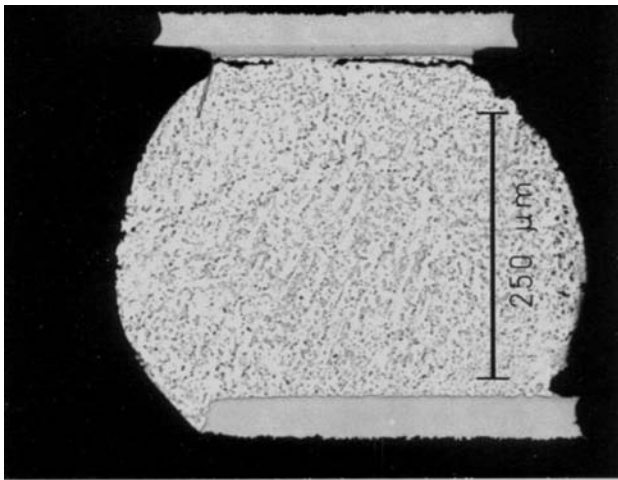


Fig. 2.35b. NEMI Lead-Free Assembly Project cross section of 169 CSP solder joint fabricated with Sn-3.9Ag-0.6Cu after ATC: -40°C to 125°C. Note that the microstructure in Fig. 2.35b is significantly coarser than Fig. 2.35a. [18]

The situation is even more complicated for accelerated thermo-mechanical cycling (ATC): during ATC, a solder joint will develop a changing composition, stress and microstructural state that varies spatially across the solder joint, resulting in changes with the number of thermal cycles, and varies with component type and position of the solder joint on the component. Typical CSP169 solder joints from the iNEMI Lead-Free Solder Project that underwent ATC at two different thermal cycling conditions are seen in Figure 2.35. The microstructures have coarsened differently as a result of the different thermal cycling conditions. [18]

2.7.2 Accelerated Thermal Cycling and Acceleration Factors

For Sn-Pb solders, there has been widespread acceptance of ATC of PWB test vehicles under specific conditions as a reliable method to assess thermo-mechanical fatigue resistance. This acceptance came from decades of industry experience relating specific thermal cycling conditions to wear-out failure in specific classes of electronic products. The microelectronics industry is just beginning to establish the practical experience relating design, product use, and ATC that took over fifty years for Sn-Pb assemblies.

The complexity of the situation with Pb-free solders was evident from the NCMS Pb-free Project in which the Pb-free solder alloys were observed to withstand different amounts, types, and rates of loading at different temperatures which are dependent upon the different coefficients of thermal expansion (CTE) and mechanical properties of the board, components, and alloys, solder joint geometry, solder microstructure, and residual stresses. [1-4] Taken together for a given alloy, these properties produce solder joint performance better for some components than eutectic Sn-Pb and worse for other components on the same board, and are likely to be different for different thermal cycling conditions.

A major remaining question is what are the proper acceleration factors for Pb-free solders, which quantify the relationship between solder composition, thermal cycling conditions, component and board materials and geometries, and useful assembly life. The current state of understanding was enunciated by Bartelo et al., in their examination of the relative performance of Sn-Pb eutectic and Pb-free solders as a function of ATC cycling conditions for a single component type, ceramic ball grid arrays (CBGA). [62] For 0°C to 100°C ATC testing with cycles times of 30 to 240 minutes, the ATC performances of CBGAs assembled with Sn-3.8Ag-0.7Cu and Sn-3.5Ag-3.0Bi (SAB) alloys were superior to those assembled with eutectic Sn-Pb CBGAs. When the thermal cycling condition was changed to -40°C to 125°C at cycle times from 42 minutes to 240 minutes, the ATC performance

of CBGAs assembled with the SAC alloy was inferior to eutectic Sn-Pb CBGAs. Using the same temperature difference as 0°C to 100°C, the performance of the SAC alloy was superior to those assembled with eutectic Sn-Pb CBGAs. Similar results were obtained for the Sn-3.5Ag-3Bi alloy, with the added complication that for -40°C to 125°C ATC test conditions, the CBGAs assembled with SAB performed better than the Sn-Pb eutectic controls for short cycle times (42 minutes), but performed worse at longer ATC cycle times (240 minutes).

These results are similar to those obtained by Swan et al. for a wider variety of components, but a smaller set of cycling conditions. [63] Considerable data on the lifetimes of solder joints in commercial products coupled with extensive ATC testing are needed before acceleration factors can begin to be quantified for even a single alloy.

Future Work

Future research on Pb-free alloys must focus on the following issues:

- high reliability applications – server, military, aerospace, medical, for which exemptions are going away or where the lack of availability of tin-lead components will force a switch to lead-free soldering
- understanding whether there are any significant differences between different SAC alloy compositions in terms of reliability
- acceleration factors for SnAgCu and SnCu based alloys
- interactions of lead-free solder alloys and board/component surface finishes (containing gold, nickel, bismuth, silver, copper)
- effects of lead-free soldering time above liquidus temperature and peak soldering temperature on intermetallic formation and solder joint microstructure and its effect on reliability
- effect of lead-free cooling rate and subsequent aging on intermetallic compound and solder joint microstructure and their effect on reliability
- copper dissolution studies with different lead-free solder joint alloys and reliability of the resulting solder joint
- effect of CuSn, NiSn, NiCuSn, AgSn, AuSn intermetallic on lead-free solder joint reliability
- effect of lead-free surface mount, wave and rework (BGA, Hand, wave) processing on intermetallic formation and solder joint microstructure with the resultant affect on reliability
- effect of lead-free wave solder holefill on reliability

- effect of ATC and mechanical testing (bend, shock, vibration) on lead-free solder joint reliability
- effect of ATC dwell time and temperature ranges on lead-free solder joint reliability

Acknowledgements

The authors gratefully acknowledge the valuable contributions of their colleagues at NIST and their industry colleagues, including Jasbir Bath, Edwin Bradley, Srinivas Chada, Nikhilesh Chawla, Jean-Paul Clech, Darrel Frear, Polina Snugovsky, and Werner Engelmeier.

References

1. NCMS Lead-Free Solder Project Final Report, NCMS, National Center for Manufacturing Sciences, 3025 Boardwalk, Ann Arbor, Michigan 48108-3266, Report 0401RE96, August 1997, and CD-ROM database of complete dataset, including micrographs and raw data, August, 1999. Information on how to order these can be obtained from: <http://www.ncms.org/>
2. I. Artaki, D. Noctor, C. Desantis, W. Desaulnier, L. Felton, M. Palmer, J. Felty, J. Greaves, C.A. Handwerker, J. Mather, S. Schroeder, D. Napp, T.Y. Pan, J. Rosser, P. Vianco, G. Whitten, and Y. Zhu. Research trends in lead-free soldering in the US: NCMS lead-free solder project (Keynote). 602-605. 1999. IEEE Computer Society. Proceedings-EcoDesign '99: First International Symposium on Environmentally Conscious Design and Inverse Manufacturing; February 1-3, 1999; Tokyo, Japan.
3. C.A. Handwerker, E.E. de Kluizenaar, K. Suganuma, F.W. Gayle, Major International Lead-Free Solder Studies, Eds., Puttlitz K.J., Stalter K.A. Handbook of Lead-Free Solder Technology and Microelectronic Assemblies. New York: Marcel Dekker. In press.
4. C.A. Handwerker, NCMS lead-free solder project: a summary of results, conclusions and recommendations. 1999. IPC. IPC Work '99: An International Summit on Lead-Free Electronics Assemblies; Proceedings; October 23-28, 1999; Minneapolis, MN.
5. F. Gayle, G. Becka, A. Syed, J. Badgett, G. Whitten, T.-Y. Pan, A. Grusd, B. Bauer, R. Lathrop, J. Slattery, I. Anderson, J. Foley, A. Gickler, D. Napp, J. Mather, C. Olson, High temperature lead-free solder for microelectronics J. Minerals, Metals & Materials Soc. 53 (6): 17-21 June 2001.
6. F.W. Gayle, Fatigue-Resistant, High Temperature Solder, Advanced Materials & Processes 159 (4), April 2001, p. 43-44.
7. F.W. Gayle, G. Becka, A. Syed, J. Badgett, G. Whitten, T.-Y. Pan, A. Grusd, B. Bauer, R. Lathrop, J. Slattery, I. Anderson, J. Foley, A. Gickler, D. Napp,

-
- J. Mather, C. Olson, High temperature lead-free solder for microelectronics, NCMS, Ann Arbor, MI, 2001 (published on CD-ROM).
8. J.H. Vincent, B.P. Richards, D.R. Wallis, I. Gunter, M. Warwick, H.A.H. Steen, P.G. Harris, M.A. Whitmore, S. Billington, A.C. Harman, and E. Knight, "Alternative solders for electronics assemblies. Part 2: UK progress and preliminary trials," *Circuit World*, 19: pp.32-34, 1993.
 9. Alternative Solders for Electronic Assemblies – Final Report of DTI Project 1991-1993, GEC Marconi, ITRI, BNR Europe, and Multicore Solders. DTI Report MS/20073, issued 10.26.93.
 10. H. Vincent and G. Humpston, "Lead-free solders for electronic assembly," *GEC Journal of Research*, 11: pp.76-89, 1994.
 11. M. Harrison and J.H. Vincent, "Improved Design Life and Environmentally Aware Manufacturing of Electronic Assemblies by Lead-Free Soldering," <http://www.lead-free.org/research/index.html>.
 12. M.R. Harrison and J. Vincent, "IDEALS: Improved design life and environmentally aware manufacturing of electronics assemblies by lead-free soldering", *Proc. IMAPS Europe '99*, (Harrogate, GB), June 1999.
 13. C.A. Handwerker, F.W. Gayle, E. de Kluizenar, K. Suganama, Major International Lead (Pb)- Free Solder Studies, in *Handbook of Lead-free Solder Technology for Microelectronics Assemblies*, Eds. K.J. Puttlitz and K.A. Stalter, Marcel Dekker, 2004.
 14. M.H. Biglari, M. Oddy, M.A. Oud, P. Davis, E.E. de Kluizenaar, P. Langeveld, and D. Schwarzbach, "Pb-free solders based on SnAgCu, SnAgBi, SnAg, and SnCu, for wave soldering of electronic assemblies," *Proc. Electronics Goes Green 2000+*, (Berlin, Germany) September 2000.
 15. J. Bath, C.A. Handwerker, E. Bradley, Research Update: Lead-Free Solder Alternatives, *Circuits Assembly*, May 2000, 31-40.
 16. E. Bradley, NEMI Pb-free interconnect task group report. 1999. *IPC Works '99: An International Summit on Lead-Free Electronics Assemblies*; Proceedings; October 23-28, 1999; Minneapolis, MN.
 17. A. Rae and C.A. Handwerker, *Circuits Assembly*, April 2004, 20-25.
 18. E. Bradley, J. Bath, C.A. Handwerker, R.D. Parker, *Lead-Free Electronics: iNEMI Projects Lead to Successful Manufacturing*, 2007, in press.
 19. K. Suganuma, Research and development for lead-free soldering in Japan. 1999. *IPC. IPC Work '99: An International Summit on Lead-Free Electronics Assemblies*; Proceedings; October 23-28, 1999; Minneapolis, MN.
 20. JEITA Lead-free Roadmap 2002 for Commercialization of Lead-free Solder, September 2002, *Lead-Free Soldering Roadmap Committee, Technical Standardization Committee on Electronics Assembly Technology*, JEITA (Japan Electronics and Information Technology Industries Association).
 21. NEDO Research and Development on Lead-Free Soldering, Report No.00-ki-17, JEIDA, Tokyo, Japan, 2000.
 22. Lead-Free Soldering – An Analysis of the Current Status of Lead-Free Soldering, Report from the UK Department of Trade and Industry. Copies can be obtained from the ITRI website: <http://www.lead-free.org/>

23. Second European Lead-Free Soldering Technology Roadmap, February 2003 and Framework for an International Lead-Free Soldering Roadmap, December 2002, Soldertec, available at <http://www.lead-free.org>.
24. ASM Binary Alloy Phase Diagrams, Eds. T.B. Massalski, H. Okamoto, P.R. Subramanian, L. Kacprzak, ASM International, 1990.
25. U.R. Kattner, Phase diagrams for lead-free solder alloys, JOM-JOURNAL OF THE MINERALS METALS & MATERIALS SOCIETY, 54 (12): 45-51, 2002.
26. U.R. Kattner, C.A. Handwerker. Calculation of phase equilibria in candidate solder alloys. Zeitschrift fur Metallkunde 2001; 92(7): 740-746.
27. K.W. Moon, W.J. Boettinger, U.R. Kattner, F.S. Biancaniello, C.A. Handwerker. Experimental and thermodynamic assessment of Sn-Ag-Cu solder alloys. Journal of Electronic Materials 2000; 29(10): 1122-1136.
28. U.R. Kattner and W.J. Boettinger, "On the Sn-Bi-Ag ternary phase-diagram," Journal of Electronic Materials 23 (1994) 603-10.
29. K.W. Moon, W.J. Boettinger, U.R. Kattner, C.A. Handwerker, D.J. Lee, The effect of Pb contamination on the solidification behavior of Sn-Bi solders, J. Elec. Mater. 30 (1): 45-52 (2001).
30. S. Chada, W. Laub, R.A. Fournelle, and D. Shangguan, Copper substrate dissolution in eutectic Sn-Ag Solder and its Effect on Microstructure, J. Electronic Mater. 29, 1214-1221 (2000).
31. T.M. Korhonen, P. Su, S.J. Hong, M.A. Korhonen, and C.-Y. Li, Reactions of Lead-Free Solders with CuNi Metallizations, J. Electronic Mater. 29 1194-1199 (2000).
32. D. Swenson, The effects of suppressed beta tin nucleation on the microstructural evolution of lead-free solder joints, J. Mater. Sci. Mater. Electronics, 18 39-54 (2007).
33. J.W. Jang and D. Frear, unpublished research.
34. JCAA/JG-PP No-Lead Solder Project: -55°C to +125°C Thermal Cycle Testing Final Project, Rockwell Collins, D. Hillman and R. Wilcoxon, May 28, 2006.
35. K.S. Kim, S.H. Huh, and K. Suganuma, Effects of cooling speed on microstructure and tensile properties of Sn-Ag-Cu alloys, Mater. Sci. Eng. A. 333 106-114 (2002).
36. D.W. Henderson, T. Gosselin, A. Sarkhel, S.K. Kang, W.K. Choi, D.Y. Shih, C. Goldsmith, and K.J. Puttlitz, Ag₃Sn plate formation in the solidification of near ternary eutectic Sn-Ag-Cu alloys, J. Mater. Res., 17 2775-2778 (2002).
37. I.E. Anderson, J.C. Foley, B.A. Cook, J. Harringa, R.L. Terpstra, O. Unal, Alloying effects in near-eutectic Sn-Ag-Cu solder alloys for improved microstructural stability, J. Electron. Mater. 30 (9): 1050-1059 (2001).
38. I.E. Anderson, B.A. Cook, J. Harringa, R.L. Terpstra, Microstructural modifications and properties of Sn-Ag-Cu solder joints induced by alloying, J. Electron. Mater. 31, 1166-1174 (2002).
39. K.L. Buckmaster, J.J. Dziejcz, M.A. Masters, B.D. Poquette, G.W. Tormoen, D. Swenson, D.W. Henderson, T. Gosselin, S.K. Kang, D.Y. Shih and K.J. Puttlitz, Presented at the TMS 2003 Fall Meeting, Chicago, IL, November, 2003.
40. M.A. Dudek, R.S. Sidhu, and N. Chawla, Novel rare-earth-containing lead-free solders with enhanced ductility, J. Metals 58 (6) 57-62 (2006).

41. K. Suganuma, Microstructural features of lift-off phenomenon in through hole circuit soldered by Sn-Bi. *Scripta Materialia* 1998; 38(9):1333-1340.
42. W.J. Boettinger, C.A. Handwerker, B. Newbury, T.Y. Pan, J.M. Nicholson, Mechanism of fillet lifting in Sn-Bi alloys, *J. Elec. Mater.*, 31 (5): 545-550 MAY 2002.
43. H. Takao, H. Hasegawa, Influence of alloy composition on fillet-lifting phenomenon in Sn-Ag-Bi alloys, *J. Elec. Mater.*, 30(2001), 513-520.
44. P. Biocca, Solder Paste: What are the process requirements to achieve reliable lead-free wave soldering?, http://www.leadfreemagazine.com/pages/papers/Q_A_Kester.pdf.
45. P. Biocca, Reliable Lead-Free Wave Soldering and SMT Processes, http://ap.pennnet.com/Articles/Article_Display.cfm?Section=Articles&Subsection=Display&ARTICLE_ID=216210.
46. K.-W. Moon, U.R. Kattner, and C.A. Handwerker, The Effect of Bi Contamination on the Solidification Behavior of Sn-Pb Solder, *J. Elec. Mater.* Nov. 2006.
47. NIST Thermodynamic Database for Solder Alloys, <http://www.metallurgy.nist.gov/phase/solder/>
48. J.-O. Andersson, T. Helander, L. Höglund, P. Shi, and B. Sundman, Thermo-Calc and DICTRA, Computational Tool for Materials Science, *Calphad* 26 (2002) 273-312.
49. W.J. Boettinger, U.R. Kattner, S.R. Coriell, Y.A. Chang and B.A. Mueller, A Development of Multicomponent Solidification Micromodels Using a Thermodynamic Phase Diagram Data Base, in *Modeling of Casting, Welding and Advanced Solidification Processes, VII*, Eds. M. Cross and J. Campbell, TMS, Warrendale, PA, 1995, 649-656.
50. D.W.G. White, Surface tensions of Pb, Sn, and Pb-Sn alloys, *Metallurgical Transactions*, 2 (1971) 3067-3071.
51. I. Ohnuma, X.J. Liu, H. Ohtani, K. Anzai, R. Kainuma, K. Ishida, Development of thermodynamic database for micro-soldering alloys, *Electronics Packaging Technology Conference, 2000. (EPTC 2000)*. Proceedings of 3rd Conference, 2000, 91-96.
52. I. Ohnuma, M. Miyashita, K. Anzai, X.J. Liu, H. Ohtani, R. Kainuma, Phase equilibria and the related properties of Sn-Ag-Cu based Pb-free solder alloys. *J. Elec. Mater.* 2000; 29(10): 1137-1144.
53. N.-C. Lee, Prospect of lead-free alternatives for reflow soldering. 1999. ICP. IPC Work '99: An International Summit on Lead-Free Electronics Assemblies; Proceedings; October 23-28, 1999; Minneapolis, MN.
54. E. Bradley and J. Hranisavljevic, ECTC, 50th Electronic Components & Technology Conference, IEEE Transactions on Electronics Packaging Manufacturing 24:4 (10/2001) 255-260.
55. J.P. Clech, Report to NIST on Review and Analysis of Lead-Free Solder Material Properties, 2002, <http://www.metallurgy.nist.gov/solder/clech/Introduction.htm>.
56. M. Kerr and N. Chawla, Creep deformation behavior of Sn-3.5Ag solder/Cu couple at small length scales, *Acta Mater.* 52 4527-4535 (2004).

57. X. Deng, N. Chawla, K.K. Chawla, and M. Koopman, Deformation behavior of (Cu,Ag)-Sn intermetallics by nanoindentation, *Acta. Mater.* 52 4291-4303 (2004).
58. F. Ochoa, X. Deng, and N. Chawla, Effects of cooling rate on creep behavior of a Sn-3.5Ag alloy, *J. Electron. Mater.* 33 1596-1607 (2004).
59. Personal Communication D. Frear and E. Bradley (2000).
60. F. Guo, S. Choi, K.N. Subramanian, T.R. Bieler, J.P. Lucas, A. Achari, M. Paruchuri, Evaluation of creep behavior of near-eutectic Sn-Ag solders containing small amounts of alloy additions, *Mater. Sci. Eng. A* 35: 190-199 (2003).
61. R. Darveaux and K. Banerji, *IEEE Trans. Components, Hybrid and Manufacturing Technology* 15 1013-1024 (1992).
62. J. Bartelo, S.R. Cain, D. Caletka, K. Darbha, T. Gosselin, D.W. Henderson, D. King, K. Knadle, A. Sarkhel, G. Thiel, C. Woychik, "Thermomechanical fatigue behavior of selected lead-free solders", *Proceedings, IPC SMTA Council APEX 2001*, Paper # LF2-2.
63. G. Swan, A. Woosley, K. Simmons, T. Koschmieder, T.T. Chong, and L. Matsushita. Development of lead-(Pb) and halogen free peripheral leaded and PBGA components to meet MSL3 at 260°C peak reflow profile. 1, 121-126. 9-11-2000. VDE Verlag. *Proceedings, Electronics Goes Green 2000+*, September 11-13, 2000, Berlin, Germany.



<http://www.springer.com/978-0-387-32466-1>

Lead-Free Soldering

Bath, J. (Ed.)

2007, XIV, 299 p., Hardcover

ISBN: 978-0-387-32466-1